

# Clustering acoustic emission data streams with sequentially appearing clusters using mixture models

Emmanuel Ramasso

*Institut FEMTO-ST (UMR CNRS 6174), Université Bourgogne Franche-Comté, Département Mécanique Appliquée, Besançon, France*

Thierry Denœux

*Université de technologie de Compiègne, CNRS, Heudiasyc, Compiègne, France  
Institut universitaire de France, Paris, France*

Gaël Chevallier

*Institut FEMTO-ST (UMR CNRS 6174), Université Bourgogne Franche-Comté, Département Mécanique Appliquée, Besançon, France*

---

## Abstract

The interpretation of unlabeled acoustic emission (AE) data classically relies on general-purpose clustering methods. While several external criteria have been used in the past to select the hyper-parameters of those algorithms, few studies have paid attention to the development of dedicated objective functions in clustering methods able to cope with the specificities of AE data. We investigate how to explicitly represent clusters onsets in mixture models in general, and in Gaussian Mixture Models (GMM) in particular. By modifying the internal criterion of such models, we propose the first clustering method able to provide, through parameters estimated by an expectation-maximization procedure, information about when clusters occur (onsets), how they grow (kinetics) and their level of activation through time. This new objective function accommodates continuous timestamps of AE signals and, thus, their order of occurrence. The method, called **GMMSEQ**, is experimentally validated to characterize the loosening phenomenon in bolted structure under vibrations. A comparison with three standard clustering methods on raw streaming data from five experimental campaigns shows that **GMMSEQ** not only provides useful qualitative information about the timeline of clusters, but also shows better performance in terms of cluster characterization. In view of developing an open acoustic emission initiative and according to the FAIR principles, the datasets and the codes are made available to reproduce the research of this paper <sup>1</sup>.

**Keywords:** Acoustic emission, clustering, onsets, continuous timestamps, loosening of bolted joints.

---



---

<sup>1</sup>Data are shared (link provided). Codes will be shared once the paper accepted. ©2021. This manuscript version is made available under the CC-BY-NC-ND 4.0 license, <https://creativecommons.org/licenses/by-nc-nd/4.0/>.

*Email addresses:* [emmanuel.ramasso@femto-st.fr](mailto:emmanuel.ramasso@femto-st.fr) (Emmanuel Ramasso), [thierry.denoeux@utc.fr](mailto:thierry.denoeux@utc.fr) (Thierry Denœux), [gael.chevallier@univ-fcomte.fr](mailto:gael.chevallier@univ-fcomte.fr) (Gaël Chevallier)

*URL:* <https://github.com/emmanuelramasso> (Emmanuel Ramasso), <https://www.hds.utc.fr/~tdenoeux/> (Thierry Denœux)

## 1. Introduction

ASTM standard E1316 [1, 2] defines Acoustic Emission (AE) as the detection of the subnanometric displacements of the surface of a material induced by the propagation of an elastic wave generated by a sudden and permanent change in the material integrity. This capability makes the AE technique particularly relevant to gain insights into the behavior of a material, a structure or an equipment under usage [3, 4, 5, 6, 7] and accounts for its wide use in applications related to material testing, Structural Health Monitoring (SHM) and process monitoring and control.

Original AE data take the form of a *data stream* recorded by sensors attached onto a structure (Figure 1). The sensors, converting the subnanometric displacements into voltage signals, have to be read continuously in order to catch all events originating from the material. The data stream is then segmented using a wave-picking algorithm with the aim to detect damage-related (non-noise) AE signals [8, 9, 10, 11, 12, 13]. In feature-based interpretation of AE signals, a *feature extraction* step is performed in which AE signals are represented in a common feature space. The set of feature vectors represents an AE dataset for a given experiment and is generally stored in an  $N \times d$  feature matrix

$$\mathbf{X} = [\mathbf{x}_1^\top, \dots, \mathbf{x}_i^\top, \dots, \mathbf{x}_N^\top] \quad (1)$$

where  $\mathbf{x}_i^\top \in \mathbb{R}^d$  is the transposed feature vector computed from the  $i$ -th AE signal. The timestamps of AE signals are their instants of occurrence and are denoted as  $t_i$  with

$$0 = t_0 < t_1 < \dots < t_i < \dots < t_N = T,$$

where  $T$  is the data stream duration. AE data have several special characteristics in terms of data processing [14]; in particular timestamps are continuous and *unequally-spaced in time*, i.e., we generally have

$$\frac{t_i - t_{i-1}}{t_j - t_{j-1}} \neq 1. \quad (2)$$

For a given AE signal, the  $d$  features generally belong to a standard list of AE features, some of which are listed, for example, in [15]. In the sequel, we suppose that the features have been extracted using the algorithm introduced in [12], which implements in MATLAB® common features available in the Mistras AEWIn® software. Unsupervised feature selection is not tackled in this paper. The reader interested in this topics can refer, for instance, to the aforementioned references and [16, 17, 18, 19].

Since a huge amount<sup>2</sup> of AE signals can be detected in a data stream, it is difficult, except for specific configurations, to know the ground truth for a sufficient large amount of AE signals. Lack of knowledge about the source of AE signals prevents us from using supervised learning methods for AE data interpretation, or even for anomaly detection when “normal” condition data are available [21, 22]. *Unsupervised learning*, particularly based on clustering, is generally used to extract information from AE data. This is the main scope of the present work.

*Clustering* methods have been applied for decades to interpret AE data. The most commonly used methods are the K-means [23, 24], the fuzzy C-means (FCM) [25, 26], the Gustafson-Kessel (GK) algorithm [27, 20] and Gaussian Mixture Models (GMM) [28, 29]. A clustering method computes membership degrees of feature vectors to clusters; a hard partition is then obtained by

---

<sup>2</sup>The number of AE signals depends on the materials and the type of loading. For example, hundreds of thousands of signals were detected for composite materials during quasi-static tests reported in [20].

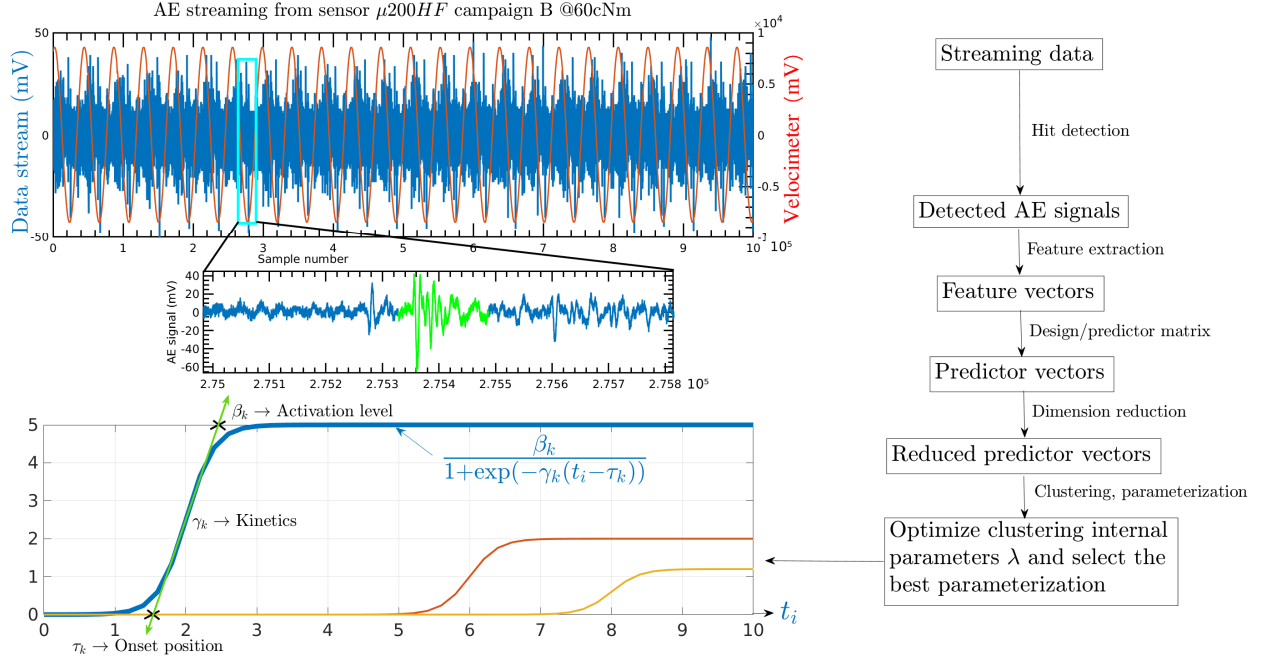


Figure 1: Proposed methodology and illustration on a real data stream extracted from one of the the datasets considered in the experiments.

assigning each vector to its maximum-membership cluster. Based on this partition, data interpretation is generally necessary to find out the correspondence between clusters and damages. From a statistical point of view, the criteria used in the classical clustering methods rely on the assumption that AE signals are *independent and identically distributed* (iid). Therefore, the partition, after applying one of those methods, does not depend on the ordering. From a physical point of view, this seems counterintuitive in most of AE-related applications since the progression of a damage type is known to depend on the preceding damage states and damage accumulation [30, 31]. To cope with this problem, we need a clustering method taking the time distribution of AE signals into account. Note that “time” can be replaced by any monotonically increasing measure such as cumulative loading or cycles.

Clustering methods dedicated to time-series have been developed in the past [32, 33] but only a few of them are able to manage continuous and uneven timestamps as shown in the recent review [34]. One of the first attempts to modify standard approaches (such as K-means, FCM or GMM) so as to accommodate temporal data with such timestamps was presented in [35]. The authors modeled the time series as piece-wise linear functions and proposed a distance measure between slopes. Using this distance, they derived a modified version of the FCM method.

Clustering methods generally used in AE rely on algorithms aiming at optimizing a set of *internal* parameters (such as the cluster centers in the case of the K-means). An *external* criterion is used to tune the hyperparameters, such as the number of clusters or the subset of features. In the majority of publications, hyperparameters are generally set by finding clusters with the best compactness and separability using external indices such as the Davies-Bouldin or Dunn indices [29, 36, 37] *without considering onsets*. In some cases, the cumulative frequency of each cluster is plotted to interpret the timeline or chronology of clusters, but with a linear-linear representation

making the analysis of the onsets secondary in the interpretation [38, 39, 40]. Indeed, results are often unreadable because some clusters have much larger rate of occurrence than others. The log-linear representation is better since it scales the magnitudes of the changing quantities while the linear horizontal axis marks off the units of time during which the changes took place [41]. This representation particularly highlights cluster onsets and is suitable to compare methods on the basis of chronology [42, 43]. In some AE-related publications, authors have considered onset times of clusters in an external criterion with the objective to set hyperparameters. The first attempt was made in [20] using consensus clustering where the authors proposed an external criterion depending on the cumulative proportions of clusters. In [44, 14], onset times were explicitly used in an external criterion to select the features and the number of clusters. However, to the best of our knowledge, *the onset times of clusters have not been considered in an internal criterion so far*. Considering onset times in the clustering objective is the main scope of the present work.

In this paper, we focus on GMM and we modify the generative model to include the fact that AE signals are indexed by continuous timestamps. More specifically, the proportions in the GMM are assumed to vary in time according to a model of evolution based on sigmoid functions (Figure 1). Each sigmoid function allows us to represent:

- The level of activation of a given damage related to the cumulative number of signals generated by this damage;
- The growth rate of the damage driven by the slope of the sigmoid function at the origin and related to the kinetics of the damage;
- The instant of the damage onset.

Therefore, this new clustering method makes it possible to identify when a damage first occurs (onset), how it grows (kinetics) and how it accumulates (cluster progression).

The ability to represent onset times, kinetics and activation level makes this approach relevant for applications in which the chronology, sequence or timeline are of key importance. Another advantage of the proposed method is that the compactness and separability of clusters in the feature space is still of primary importance because it is managed explicitly using a mixture model with the possibility to adapt the distribution to the data. While being developed to take AE data characteristics into account, this new clustering method can be applied to other temporal data for which onsets, growths and cumulative progression of clusters are relevant to the analysis. The proposed optimization procedure assumes that all data are available at once (offline analysis).

As will be presented in Section 2, the parameters of the proposed method are automatically estimated from the data using an Expectation-Maximisation (EM) procedure. The method is illustrated in Section 3 using both simulated data and a real dataset collected during SHM experiments. In view of developing an open acoustic emission initiative and according to the FAIR principles, the datasets and the codes are made available to reproduce the research of this paper. Datasets are described in a co-submission in Data-in-Brief journal [45] and share on Dataverse [46], while the codes are shared on Github<sup>3</sup>.

---

<sup>3</sup>The project will be made publicly available at <https://github.com/emmanuelramasso/GMMSEQ> once the paper accepted.



## 2. Gaussian Mixture Model with sequentially appearing clusters (GMMSEQ)

The GMMSEQ method introduced in this paper is based on a GMM with time-varying proportions. The model will be described in Section 2.1, and parameter estimation will be addressed in Section 2.2.

### 2.1. Model

*Gaussian mixture models.* In a mixture model, the data are supposed to follow a probability distribution defined as a weighted sum of  $K$  distributions:

$$p(\mathbf{x}_i; \boldsymbol{\theta}) = \sum_{k=1}^K \pi_k g(\mathbf{x}_i; \boldsymbol{\theta}), \quad (3)$$

where  $\pi_k$  denotes the proportion of component  $k$  and  $g$  can be, for example, a Gaussian, Gamma or Student-t probability density function (pdf); the vector of all parameters is represented by  $\boldsymbol{\theta}$ . In AE data clustering, GMM's [28] have been widely used [29, 47, 48, 49, 50, 22] and are considered in the following developments. Each component in the mixture (3) is then a Gaussian pdf:

$$\phi(\mathbf{x}_i; \boldsymbol{\mu}_k, \boldsymbol{\Sigma}_k) = \frac{1}{\sqrt{(2\pi)^d |\boldsymbol{\Sigma}_k|}} \exp \left( -\frac{1}{2} (\mathbf{x}_i - \boldsymbol{\mu}_k)^T \boldsymbol{\Sigma}_k^{-1} (\mathbf{x}_i - \boldsymbol{\mu}_k) \right), \quad (4)$$

where  $\boldsymbol{\mu}_k$  and  $\boldsymbol{\Sigma}_k$  are, respectively, the mean and covariance matrix of component  $k$ .

Under the iid assumption, the likelihood function is

$$L(\boldsymbol{\theta}; \mathbf{x}_1, \dots, \mathbf{x}_N) = \prod_{i=1}^N \sum_{k=1}^K \pi_k \phi(\mathbf{x}_i; \boldsymbol{\mu}_k, \boldsymbol{\theta}_k), \quad (5)$$

where  $\boldsymbol{\theta} = (\boldsymbol{\mu}_1, \dots, \boldsymbol{\mu}_K, \boldsymbol{\Sigma}_1, \dots, \boldsymbol{\Sigma}_K, \pi_1, \dots, \pi_{K-1})$ . The maximum likelihood estimates (MLE's) cannot be computed in closed form and are usually computed numerically using the EM algorithm [51].

*New model.* We propose to modify (5) in order to incorporate a time-dependency of the data through the proportions:

$$p(\mathbf{x}_1, \dots, \mathbf{x}_N; \boldsymbol{\theta}) = \prod_{i=1}^N \sum_{k=1}^K \pi_{ik} \phi(\mathbf{x}_i; \boldsymbol{\mu}_k, \boldsymbol{\Sigma}_k), \quad (6)$$

where the bold subscript in  $\pi_{ik}$  emphasizes the difference with (5), i.e., the proportion of each cluster  $k$  are now dependent on the timestamps  $t_i$  through additional variables  $\alpha_{ik}$ :

$$\pi_{ik} = \frac{\alpha_{ik}}{\sum_{\ell=1}^K \alpha_{i\ell}}, \quad k = 1, \dots, K, \quad (7)$$

where  $\alpha_{i1} = 1$  for  $i = 1, \dots, N$  and

$$\alpha_{ik} = \frac{\beta_k}{1 + \exp[-\gamma_k(t_i - \tau_k)]}, \quad k = 2, \dots, K, \quad i = 1, \dots, N. \quad (8)$$

Parameters  $\tau_k$ ,  $\beta_k$  and  $\gamma_k$  in the logistic (sigmoid) activation functions (8) must satisfy the following constraints:

$$0 \leq \tau_k \leq T, \quad \beta_k \geq 0, \quad \gamma_k \geq 0 \quad (9)$$

for  $k = 2, \dots, K$ . As illustrated in Figure 1 (bottom-left), the degree of activation  $\alpha_{ik}$  of the  $k$ -th cluster depends on the real timestamps of AE signals through a sigmoid function delayed by  $\tau_k$ , with upper limit  $\beta_k$  and slope  $\gamma_k$ . The delay  $\tau_k$  represents the onset time of cluster  $k$ . The proportions  $\pi_{ik}$  in (7) are equal to the normalized activation degrees. An example of how proportions can vary in time is shown in Figure 5b.

## 2.2. Parameter estimation

Maximum-likelihood parameter estimation in GMM's is usually carried out using the EM algorithm [52], an approach that will also be used here. However, update equations for parameters  $\tau_k$ ,  $\beta_k$  and  $\gamma_k$  are not available, which will make it necessary to use a gradient-based optimization procedure in the M-step of the EM algorithm.

The first step is to write down the complete-data log-likelihood function for our model, as described in [53, Chap. 9]. We have

$$\ell_c(\boldsymbol{\theta}) = \sum_{i=1}^N \sum_{k=1}^K y_{ik} \log \pi_{ik} + y_{ik} \log \phi(\mathbf{x}_i; \boldsymbol{\mu}_k, \boldsymbol{\Sigma}_k), \quad (10)$$

where  $\boldsymbol{\theta} = (\{\boldsymbol{\mu}_k, \boldsymbol{\Sigma}_k\}_{k=1}^K, \{\tau_k, \beta_k, \gamma_k\}_{k=2}^K)$  is the parameter vector, and the  $y_{ik}$ 's are binary cluster-membership indicator variables such that  $y_{ik} = 1$  if observation  $i$  belongs to  $k$ , and  $y_{ik} = 0$  otherwise. Here, variables  $y_{ik}$  are missing. At each iteration  $q$  of the EM algorithm, we thus replace  $\ell_c$  by its conditional expectation given the observed data, which yields the so-called *auxiliary function*  $Q$  [51]:

$$Q(\boldsymbol{\theta}, \boldsymbol{\theta}^{(q)}) = \underbrace{\sum_{i=1}^N \sum_{k=1}^K y_{ik}^{(q)} \log \pi_{ik}}_{Q_1} + \underbrace{\sum_{i=1}^N \sum_{k=1}^K y_{ik}^{(q)} \log \phi(\mathbf{x}_i; \boldsymbol{\mu}_k, \boldsymbol{\Sigma}_k)}_{Q_2}, \quad (11)$$

with  $y_{ik}^{(q)} = \mathbb{E}_{\boldsymbol{\theta}^{(q)}}[Y_{ik} | \mathbf{x}_i]$ .

We can observe that the term  $Q_2$  on right-hand side of (11) is identical to that of the auxiliary function for a standard GMM (5) with fixed proportions, for which parameter updates that maximizes  $Q(\boldsymbol{\theta}, \boldsymbol{\theta}^{(q)})$  are known (and recalled below). The only difference between our EM procedure and the usual one for GMM's thus resides in the maximization of the first term  $Q_1$  with respect to the parameters defining the proportions  $\pi_{ik}$ . This procedure is detailed below.

*E-step.* In the E-step, we compute the conditional expectations  $y_{tk}^{(q)}$  from the current parameter values as [28]:

$$y_{ik}^{(q)} = \frac{\phi(\mathbf{x}_i; \boldsymbol{\mu}_k^{(q)}, \boldsymbol{\Sigma}_k^{(q)}) \pi_{ik}^{(q)}}{\sum_{l=1}^K \phi(\mathbf{x}_i; \boldsymbol{\mu}_l^{(q)}, \boldsymbol{\Sigma}_l^{(q)}) \pi_{il}^{(q)}} \quad (12)$$

with  $\phi$  given by (4).

*M-step for  $\boldsymbol{\mu}_k$  and  $\boldsymbol{\Sigma}_k$ .* In the M-step, parameters  $\boldsymbol{\mu}_k$  and  $\boldsymbol{\Sigma}_k$  are first updated by maximizing  $Q_2$ . The update equations are [28]:

$$\boldsymbol{\mu}_k^{(q+1)} = \frac{1}{N_k} \sum_i y_{ik}^{(q)} \mathbf{x}_i, \quad (13)$$

with  $N_k = \sum_i y_{ik}^{(q)}$ , and

$$\boldsymbol{\Sigma}_k^{(q+1)} = \frac{1}{N_k} \sum_i y_{ik}^{(q)} (\mathbf{x}_i - \boldsymbol{\mu}_k^{(q+1)})(\mathbf{x}_i - \boldsymbol{\mu}_k^{(q+1)})^\top. \quad (14)$$

*M-step for  $\tau_k$ ,  $\beta_k$  and  $\gamma_k$ .* Since no explicit update equations for parameters  $\tau_k$ ,  $\beta_k$  and  $\gamma_k$  can be obtained, they need to be updated by an iterative optimization procedure. To enforce the constraints (9), we first introduce the following auxiliary variables:

$$\tau_k = \frac{T}{1 + \exp(-\xi_k)}, \quad \beta_k = b_k^2, \quad \gamma_k = g_k^2. \quad (15)$$

The calculation of the derivatives of  $Q_1$  with respect to  $\xi_k$ ,  $b_k$  and  $g_k$  is detailed in Appendix A. We can then use any unconstrained nonlinear optimization procedure. In the experiments reported in Section 3, we used a trust region algorithm implemented in the MATLAB 2020b Optimization toolbox.

*Regularisation of the  $\tau_k$ 's.* In the considered application related to acoustic emission data clustering, physical knowledge can be available suggesting when, in the timeline of a test, some damages must have occurred. This information can be provided, for example, as prior values  $\tau_k^{\text{prior}}$  for  $\tau_k$  (for some or all  $k$  depending on the application). In this case, the auxiliary function (11) can be replaced by a regularised version

$$Q_r(\boldsymbol{\theta}, \boldsymbol{\theta}^{(q)}) = Q(\boldsymbol{\theta}, \boldsymbol{\theta}^{(q)}) - \lambda \|\boldsymbol{\tau} - \boldsymbol{\tau}^{\text{prior}}\|_2^2, \quad (16)$$

where  $\lambda$  is a regularization coefficient,  $\|\cdot\|$  is the  $L_2$  norm and  $\boldsymbol{\tau}$  is the vector of  $\tau_k$ 's for which a prior value is available.

### 3. Experiments

The GMMSEQ method is first illustrated on a toy dataset in Section 3.1. It is then applied to real experimental data from a mechanical system in Section 3.2.

#### 3.1. Simulated dataset

*Model for data generation.* A simulated dataset was generated from the following model with  $K = 4$  clusters:

$$\boldsymbol{\mu}_1 = [1 \quad 1], \quad \boldsymbol{\mu}_2 = [2 \quad 3], \quad \boldsymbol{\mu}_3 = [3 \quad 5], \quad \boldsymbol{\mu}_4 = [5 \quad 6],$$

and

$$\boldsymbol{\Sigma}_1 = \begin{bmatrix} 0.3 & 0.2 \\ 0.2 & 0.2 \end{bmatrix}, \quad \boldsymbol{\Sigma}_2 = \begin{bmatrix} 0.3 & 0.2 \\ 0.2 & 0.2 \end{bmatrix}, \quad \boldsymbol{\Sigma}_3 = \begin{bmatrix} 0.2 & 0.1 \\ 0.1 & 0.3 \end{bmatrix}, \quad \boldsymbol{\Sigma}_4 = \begin{bmatrix} 0.2 & 0.1 \\ 0.1 & 0.2 \end{bmatrix}.$$

The numbers of observations in the four clusters were set to [1000, 1000, 3000, 1000] and the timestamps were generated randomly from a uniform distribution

$$t_i = t_{i-1} + \mathcal{U}_{[0,1]},$$

starting from  $t_1 = 0$ . The value of  $T$  is thus  $\max_i t_i$  and the length of the data is equal to 6000. The parameters defining the time-varying proportions were set as follows:

$$\beta = [2.72 \quad 10.1 \quad 30.2], \quad \gamma = [0.009 \quad 0.015 \quad 0.012],$$

and the  $\tau_k$  were initialized to the time stamps  $t_i$  with  $i \in \{488, 1990, 2472\}$ .

Because the proportions in this model vary with time, the mixture density also depends on time. Contours of the mixture density are depicted in Figure 2 at four different time steps showing the gradual emergence of the four clusters. Figure 3 shows a contour plot of the likelihood function (assuming the correct number of clusters) as a function of  $\beta_4$  and  $\gamma_4$ , with the other parameters fixed at their maximum likelihood estimates.

*Model selection.* In practice, we need a criterion allowing us to select the number of clusters automatically. For mixture models, common choices are the Akaike Information Criterion (AIC), the Bayesian Information Criterion (BIC) and the Integrated Completed Likelihood (ICL) [54, 55]. We used these three criteria to select the best GMMSEQ model for the simulated data. For each run, the model was initialized by:

1. A standard GMM (with a Matlab 2020b implementation provided in the Statistics and Machine Learning Toolbox);
2. The K-means algorithm (provided in the same toolbox as for GMM);
3. A segmentation of the data into  $K$  blocks of the same size and a Gaussian distribution fitted to each block.

For the three types of initialization, 10 runs were performed for a number of clusters varying from 2 to 10. After convergence, for each number of clusters, the best run was selected according to the value of likelihood computed by (6). The values of AIC, BIC and ICL were finally computed for each model. The criteria are plotted against the number  $K$  of clusters in Figure 4. AIC shows an evolution presenting an “elbow” from which the number of clusters can be chosen, while BIC and ICL have a minimum for the correct number of clusters ( $K = 4$ ). For ICL, depending on the runs, the evolution can show several local minima as in the figure or a single one, but the global minimum is always located at the correct value. For different runs, BIC and AIC showed a consistent elbow-shaped behavior with a minimum that can be more or less pronounced for the correct number of clusters. This study with simulated data suggests that the three criteria have the ability to provide the correct number of clusters.

*Onset estimation.* In the introduction, we motivated this work by the need to process data with continuous timestamps and we proposed a model including an estimation of the onsets of clusters. The time-varying proportions ( $\pi_{ik}$ ) are represented in Figure 5 using the true values of parameters, the estimated ones, and the values used in the initialization of GMMSEQ. It can be observed that the estimated proportions are very close to the true ones.

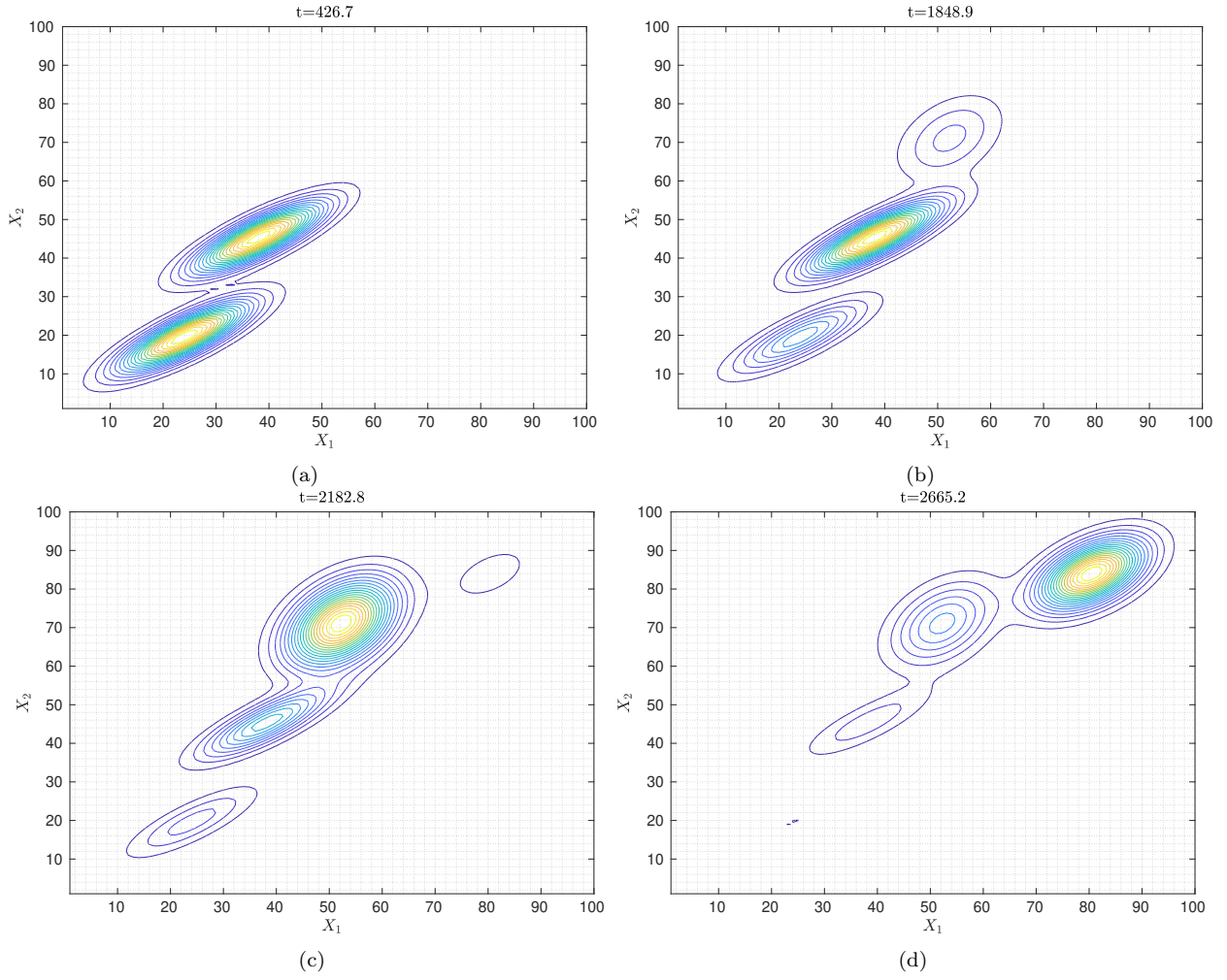


Figure 2: Contours of the mixture density at four successive time steps. The corresponding proportions  $\pi_{ik}$  correspond to the locations of the square markers in Figure 5.

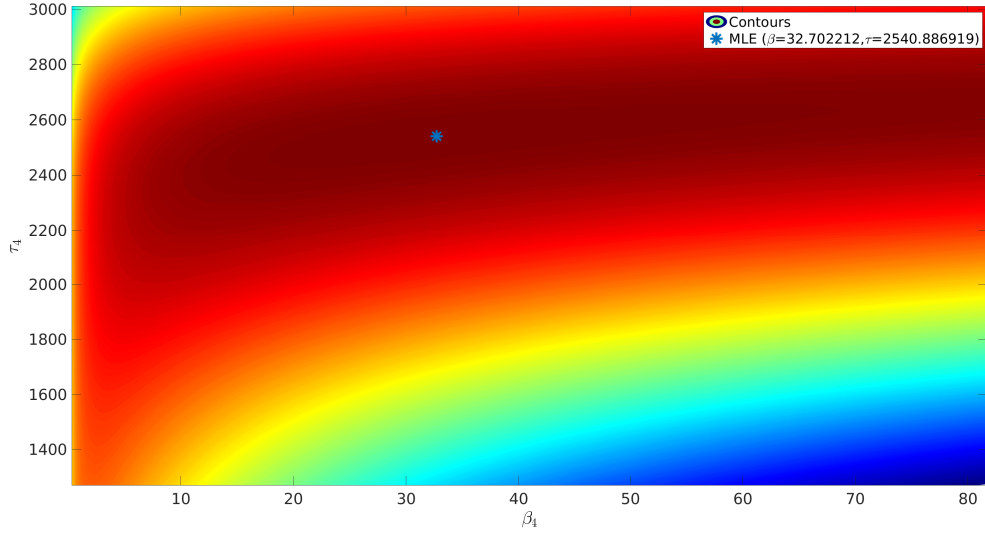


Figure 3: Contours of the log-likelihood in the plane  $(\beta_4, \gamma_4)$ , the other parameters being fixed to their maximum likelihood estimates.

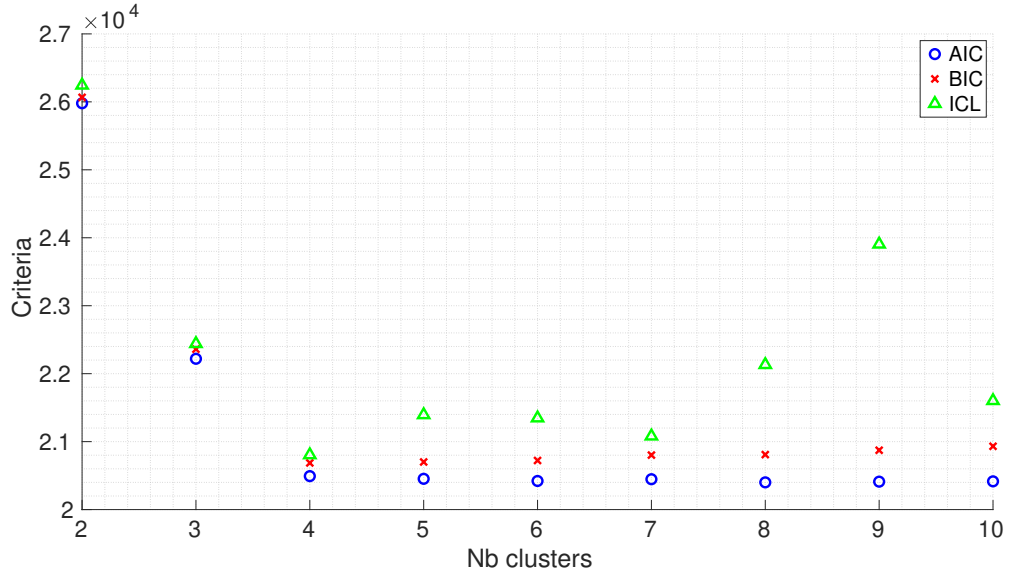
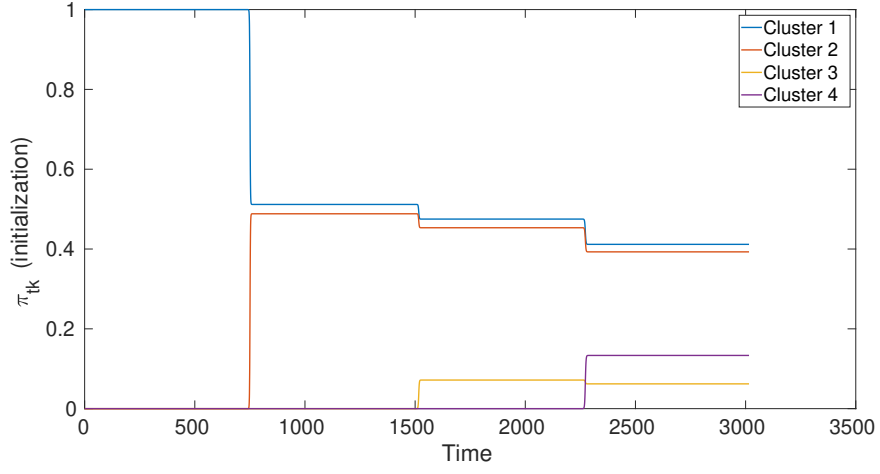
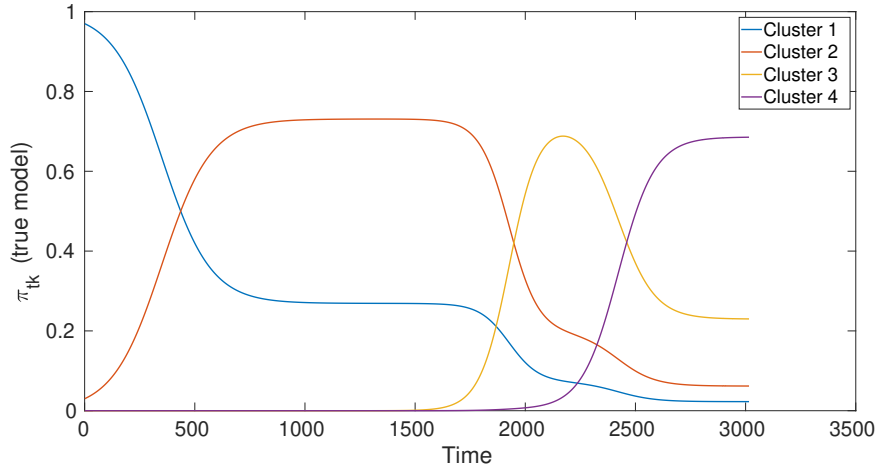


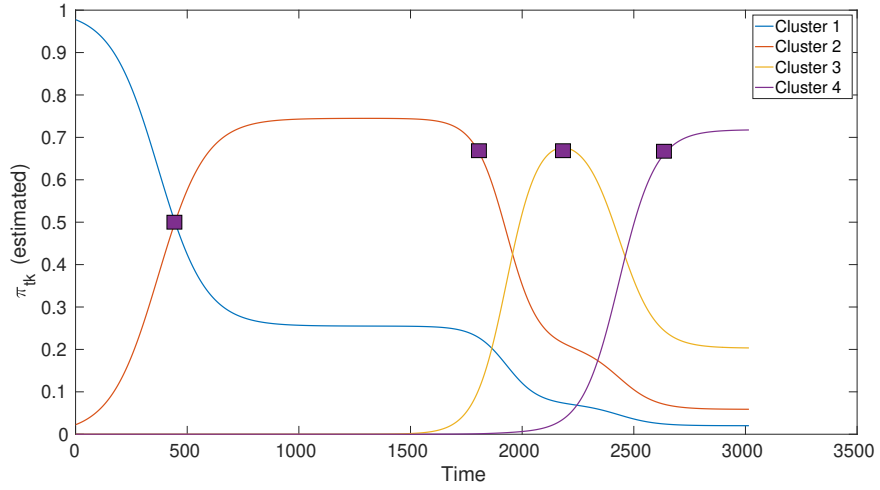
Figure 4: AIC, BIC and ICL of GMMSEQ models with different numbers of clusters for the simulated data.



(a) Initialization.



(b) True values.



(c) Estimated values.

Figure 5: Evolution of the proportions  $\pi_{ik}$  as a function of time. Squared-shape markers represent the values used in Figure 2.

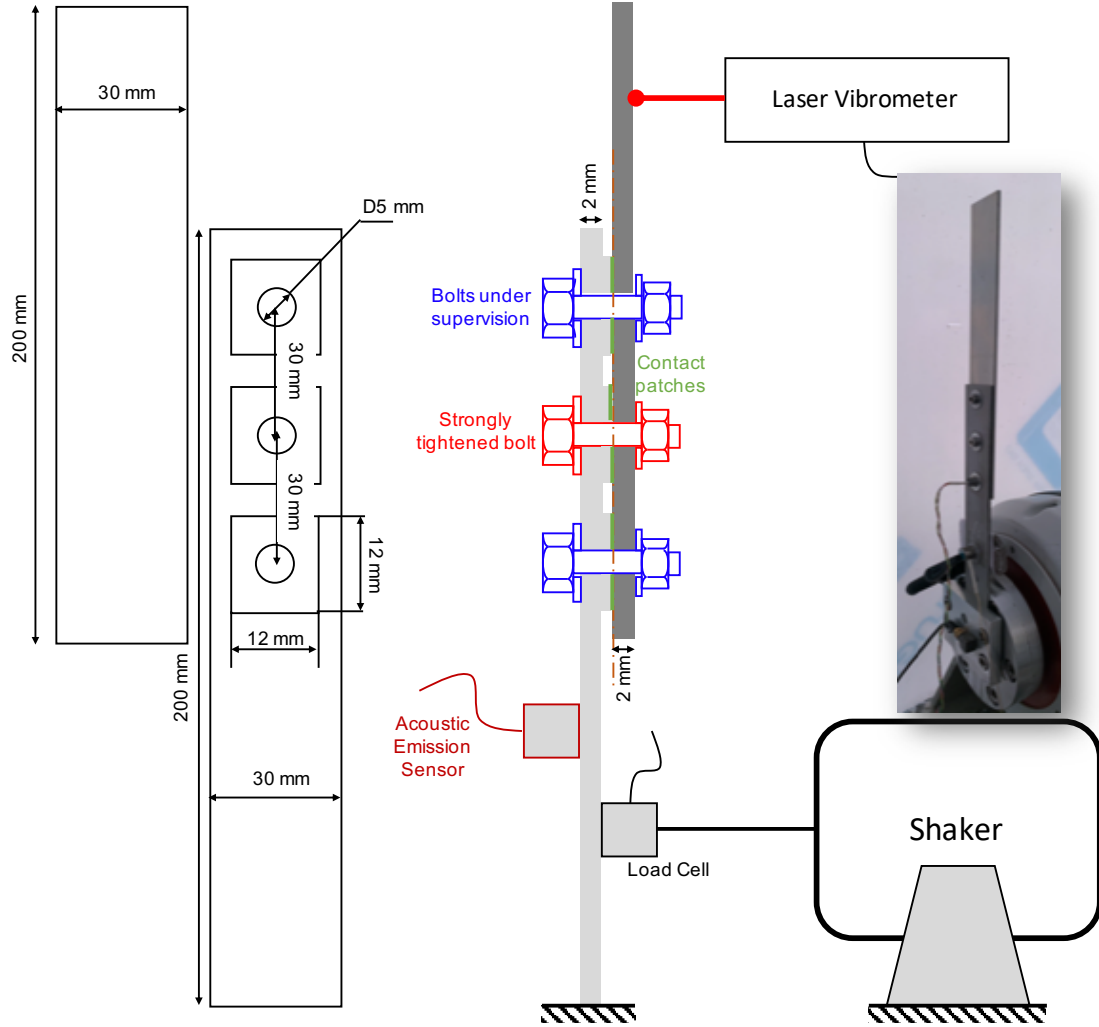


Figure 6: Setup description: part dimensions, sensor and bolt positions.

### 3.2. Real data

#### 3.2.1. Dataset description

The benchmark dataset ORION-AE [46] is used in this section to demonstrate the performance of the GMMSEQ method. The experiments<sup>4</sup> were designed to reproduce the loosening phenomenon observed in aeronautics, automotive or civil engineering structures where parts are assembled together by means of bolted joints (Figure 6). The bolts can indeed be subject to self-loosening under vibrations. Therefore, it is of paramount importance to develop sensing strategies and algorithms for early loosening estimation [57]. The test rig was specifically designed to make the vibration tests as repeatable as possible.

<sup>4</sup>This setup was initially developed to study nonlinear vibrations in the CLIMA project founded by the *Fonds Unique Interministériel* [56]. Here, we used a new set of measurements, referred to as ORION-AE, collected during the COALESCENCE project founded by the *Agence Nationale de la Recherche* and the *Institut de Recherche Technologique*.



The ORION-AE dataset is composed of five parts collected during five campaigns of measurements denoted as  $B$ ,  $C$ ,  $D$ ,  $E$  and  $F$  in the sequel. ORION is a simple jointed structure made of two plates manufactured in a 2024 aluminium alloy, linked together by three bolts. The contact between the plates is done through machined overlays. The contact patches have an area of  $12 \times 12 \text{ mm}^2$  and are 1 mm thick. The structure was submitted to a 100 Hz harmonic excitation force during about 10 seconds. The load was applied using a Tyra electromagnetic shaker, which can deliver a 200 N force. The force was measured using a PCB piezoelectric load cell and the vibration level was determined next to the end of the specimen using a Polytec laser vibrometer. Seven tightening levels were applied on the upper bolt. The tightening was first set to 60 cNm with a torque screwdriver. After a 10 seconds vibration test, the shaker was stopped and this vibration test was repeated after a torque modification at 50 cNm. Torque modifications at 40, 30, 20, 10 and 5 cNm were then applied. Note that, for campaign  $C$ , the level 20 cNm is missing. All dimensions are detailed in Figure 6 to enable readers to reproduce the test.

For each campaign, four sensors were used: a laser vibrometer and three different AE sensors (micro-200-HF, micro-80 and the F50A from Euro-Physical Acoustics) with various frequency bands were attached onto the lower plate (5 cm above the end of the plate). All data were sampled at 5 MHz using a Picoscope 4824 and a preamplifier (from Euro-Physical Acoustics) set to 60 dB. The velocimeter was used for different purposes, in particular to control the amplitude of the displacement of the top of the upper beam so that it remains constant whatever the tightening level. The sensors are expected to detect the stick-slip transitions or shocks in the interface that are known to generate small AE events during vibrations. The acoustic waves generated by these events are highly dependent on bolt tightening. These sources of AE signals have to be detected and identified from the data stream, which constitutes the challenge.

AE datasets are generally unlabeled because it is not possible to identify the AE source with certainty. This is also the case for the ORION-AE dataset. Even though we know the tightening level (1, 2 ... 7) for a period of about 10 seconds, it would be questionable to use this piece of information as a prior to train supervised methods. Indeed, different sources can be activated within the contact between the beams, in addition to shocks during vibrations which can generate signals. During each cycle of the vibration test for a given tightening level, different AE sources can generate signals and those sources may be activated or not, depending on the tribological conditions within the contact between the beams. In this paper, we assume no prior knowledge and let the algorithm find the most natural clusters. Results presented hereafter show that the content of AE signals in those campaigns allows GMMSEQ to discriminate between the periods, which seem to corroborate that the AE sources have indeed a signature depending on the tightening level.

### 3.2.2. Signal processing

The AE signals were detected from the raw data stream using a method developed in [12]. It is based on wavelet denoising (see Figure 1) used to find the onset of AE signals. The features are then extracted from the raw data stream. A compensation of the delay introduced by the filtering was performed by a number of samples equals to the number of coefficients in the wavelet. The features extracted from those detected signals are also described in [12]; they are: rise time, counts, PAC-energy, duration, amplitude, average frequency, RMS, average signal level, counts to peak, reverberation frequency, initiation frequency, signal strength, absolute energy, partial power in the intervals [0, 20, 100, 200, 300, 400, 500, 600, 800, 1000] kHz, frequency centroid, peak frequency, weighted peak frequency. To this set of features were added the following ones: the Renyi number calculated from the scalogram [58] using a Morlet wavelet, as well as the frequency of the maximum

Table 1: Some statistics about the feature extraction step (sensor  $\mu 200HF$ ).

Campaign	B	C	D	E	F
# of tightening levels	7	6	7	7	7
# features before PCA	32	32	32	32	32
# features after PCA	16	17	16	23	25
Total # of signals	10,866	9,461	9,285	15,628	17,810
Average # of signals per period	1.55	1.57	1.33	2.23	2.54

of energy in the scalogram.

We used the parameters of the method proposed in [12], i.e., hit definition time set to  $1100\ \mu s$ , hit lockout time to  $80\ \mu s$ , peak definition time to  $30\ \mu s$  and a threshold on amplitude for hit start (after denoising) set to 1.2 mV. As advised in [12], the wavelet was set to a Daubechies “dB45” made of 90 coefficients, together with 14 levels of decomposition in order to detect the onset of AE signals. The soft Donoho-Johnstone universal threshold was applied on wavelet coefficients with a rescaling using a level-dependent estimation of level noise. The data were also prefiltered using a high-pass filter of order 5 with a band-pass frequency set to 10 kHz and a band-pass ripple equal to 0.2 dB. This prefiltering allows to remove the DC component of the data stream.

Figure 7 depicts the onset of AE signals superimposed onto vibrometer data for measurement B. With the proposed settings (Fig. 7a), about 1-2 signals per cycle are found in this sample of about 1 s. We can observe that the onsets are generally positioned on a similar displacement level (measured by the vibrometer) which validates the hit detection procedure. The vibrometer data are thus useful to tune the signal processing step. It also allows us to interpret the onset of AE signals in terms of displacement necessary to trigger the related AE source.

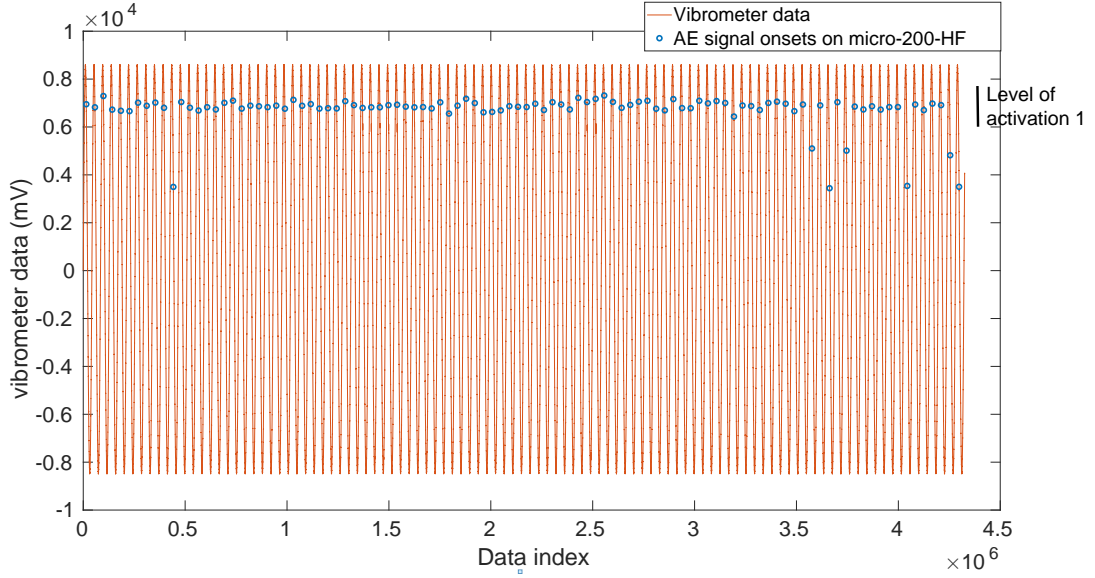
By decreasing hit definition, lockout and definition thresholds, we can find, as depicted in Figure 7b, 3-5 signals per cycle. Their onsets are now positioned according to multiple levels of displacement that trigger their source. Therefore, by modifying the thresholds, the data could become multimodal since one tightening level could be described by multiple signals with possibly different signatures.

In the sequel, the *same setting* (detailed above) was used for the signal processing step for all measurement series (B-F). With the 100 Hz harmonic vibration, Table 1 shows that about 1-2 signals on average are found per cycle for measurements B, C, D, and about 2-3 for E and F.

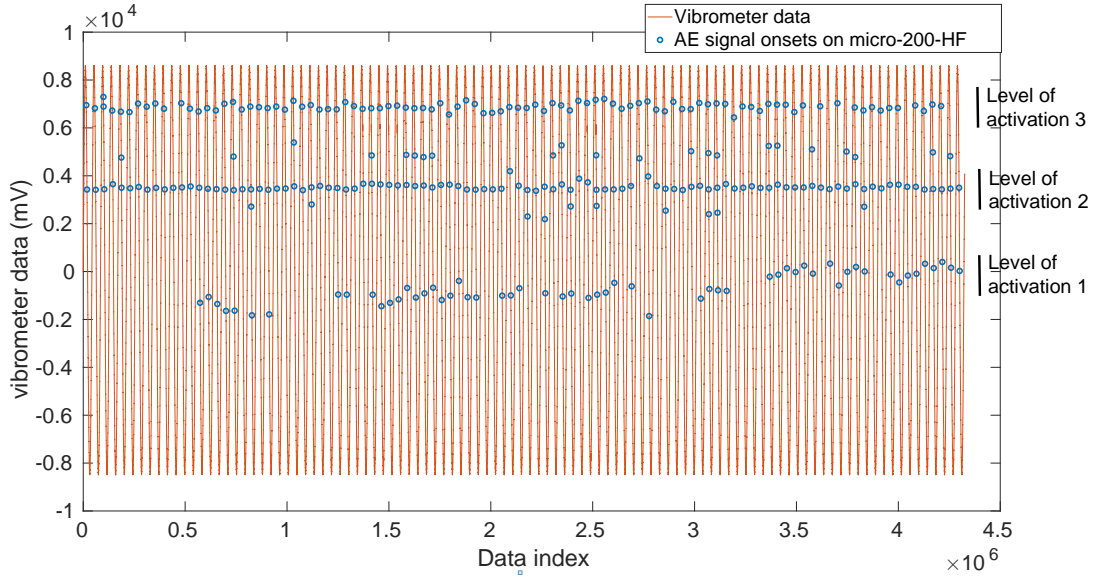
A simple 31-sample moving median was applied to each dimension of the resulting feature matrix to ensure temporal coherence. Principal Components Analysis (PCA) was used to extract the  $n$  first components explaining 99% of the variance. The value of  $n$  varies for the different campaigns as shown in Table 1, where sensor micro-200-HF was used. Figure 8 displays the first two components for campaign *E* and sensor micro-200-HF; the colors are related to the level of loosening.

### 3.3. Results

We ran the algorithm 10 times for each of the same three initialization methods mentioned in Section 3.1. The number of clusters was varied from 4 to 14. For each number of clusters, the parameter estimates corresponding to the highest likelihood were selected.



(a) With hit definition time set to  $1100 \mu s$ , hit lockout time to  $80 \mu s$ , peak definition time to  $30 \mu s$ .



(b) With hit definition time set to  $80 \mu s$ , hit lockout time to  $20 \mu s$ , peak definition time to  $20 \mu s$ .

Figure 7: Position of onset of acoustic emission signals onto vibrometer data (for measurements B,  $60 \text{ cNm}$ , first file of the dataset, using micro-200-HF sensor).

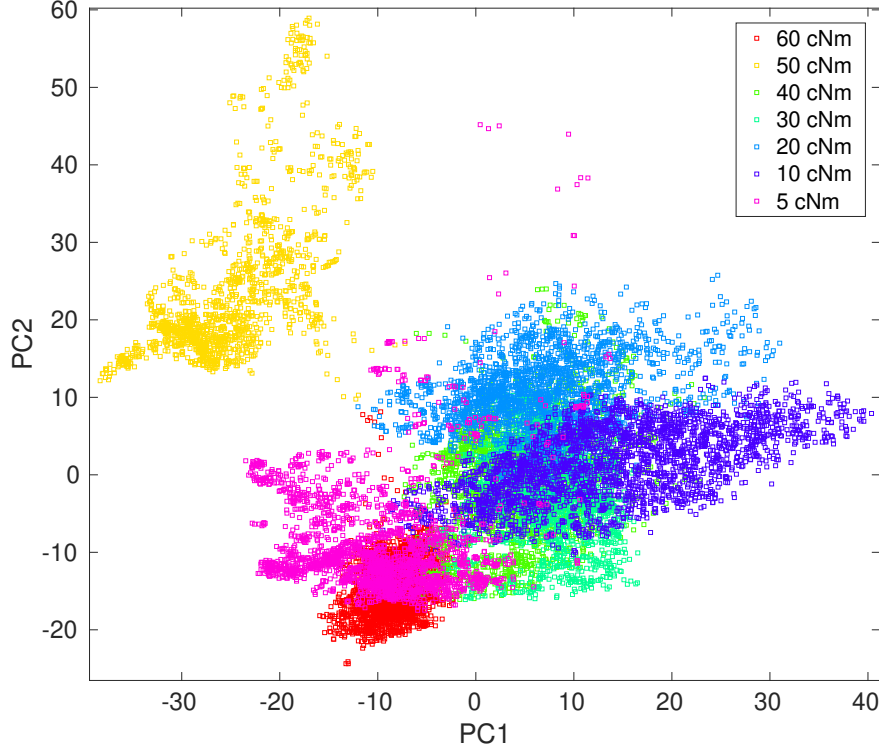


Figure 8: First two principal components of campaign *E* data.

In Section 1, we discussed the importance of the onsets in the analysis of AE dataset (represented by  $\tau_k$  in **GMMSEQ**). These values were stacked for each campaign, independently of the type of initialization or the number of clusters. Figures 9 to 13 show, in **blue**, the normalised histograms of onsets estimated by **GMMSEQ** for each campaign. The dashed lines represent the instant when the tightening level was changed. These lines are separated by about 10 s (duration of each period) for each level; therefore, the horizontal axis, which represents time, can also be related to the tightening level: 0 s to 10 s corresponding to 60 cNm, 10 s to 20 s corresponding to 50 cNm, and so on until 60 to 70 s for 5 cNm (see Figure 14). The **red** bars represent the histograms when a prior on onsets is integrated through (16) for  $K=7$  clusters.

In Figures 9 to 13, a peak in the histogram means that several models provided similar values for  $\tau_k$ . Note that there are, for the **blue** bars,  $\sum_{k=4}^{14} k = 99$  estimates of the  $\tau_k$  values, whereas there are  $K = 7$  values of  $\tau_k$  for the **red** bars. In the latter case, we can observe that the prior on onsets, taken into account in the auxiliary function, allows us to get the values of  $\tau_k$  approximately equal to the ground truth (dashed lines) for all datasets and all tightening levels. The **red** bars depict a uniform distribution since the  $\tau_k$  values are all different (after normalization, we get  $1/7$  for each estimate).

For the purely unsupervised setting (in **blue**), we can observe that the values of  $\tau_k$  with the highest probability generally correspond to the instants where a change was made on the tightening level. This observation shows that **GMMSEQ** is able to discover the levels of tightening from the features. For each campaign we can make the following comments, remembering that the levels were approximately equal to 60 (cluster 1), 50 (cluster 2), 40 (cluster 3), 30 (cluster 4), 20 (cluster 5), 10 (cluster 6) and 5 cNm (cluster 7):

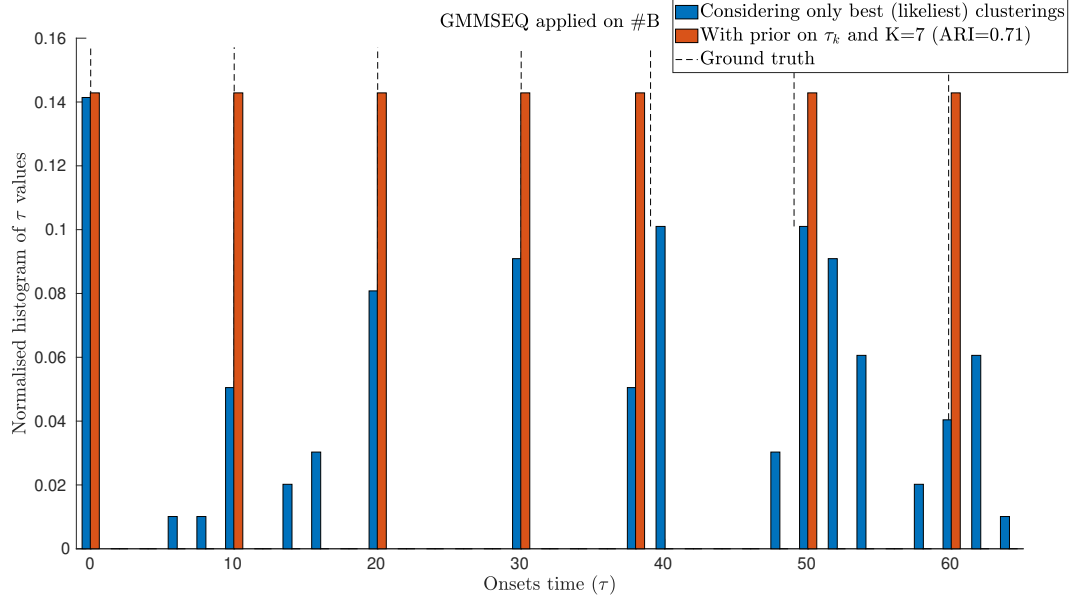


Figure 9: Campaign B: (blue) Histogram of  $\tau_k$  estimates for the three initialization methods and  $K$  ranging from 4 to 14, and (red) histogram with prior on onsets with regularization.

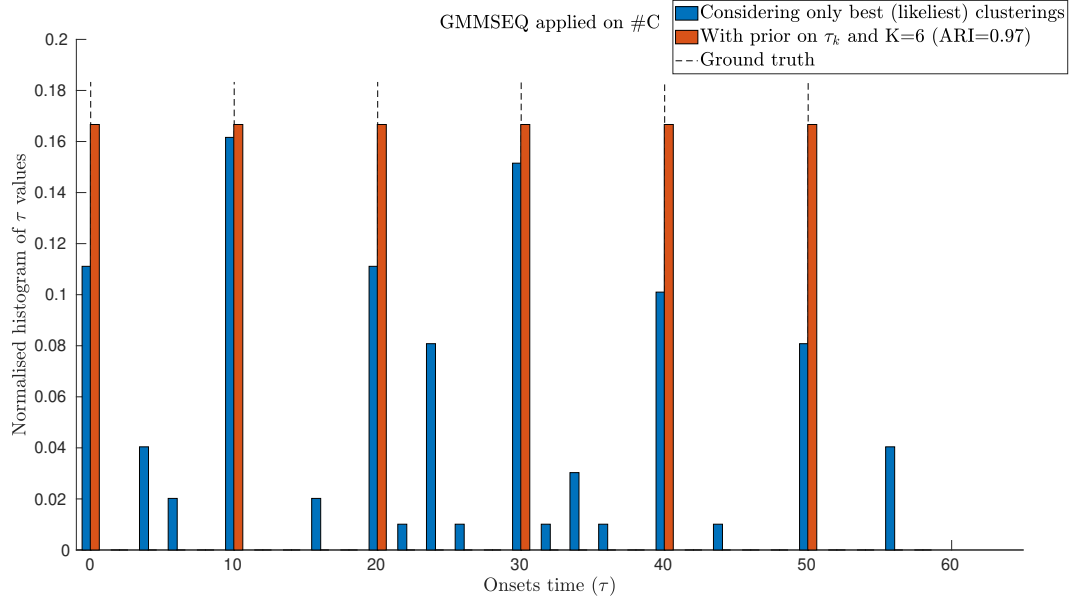


Figure 10: Campaign C: (blue) Histogram of  $\tau_k$  estimates for the three initialization methods and  $K$  ranging from 4 to 14, and (red) histogram with prior on onsets with regularization.

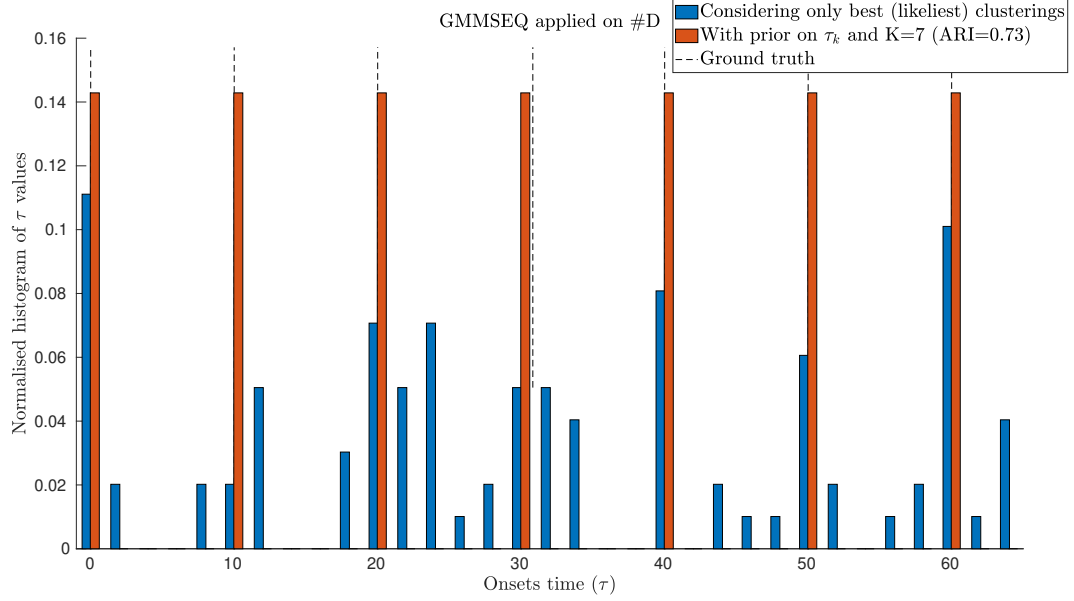


Figure 11: Campaign D: (blue) Histogram of  $\tau_k$  estimates for the three initialization methods and  $K$  ranging from 4 to 14, and (red) histogram with prior on onsets with regularization.

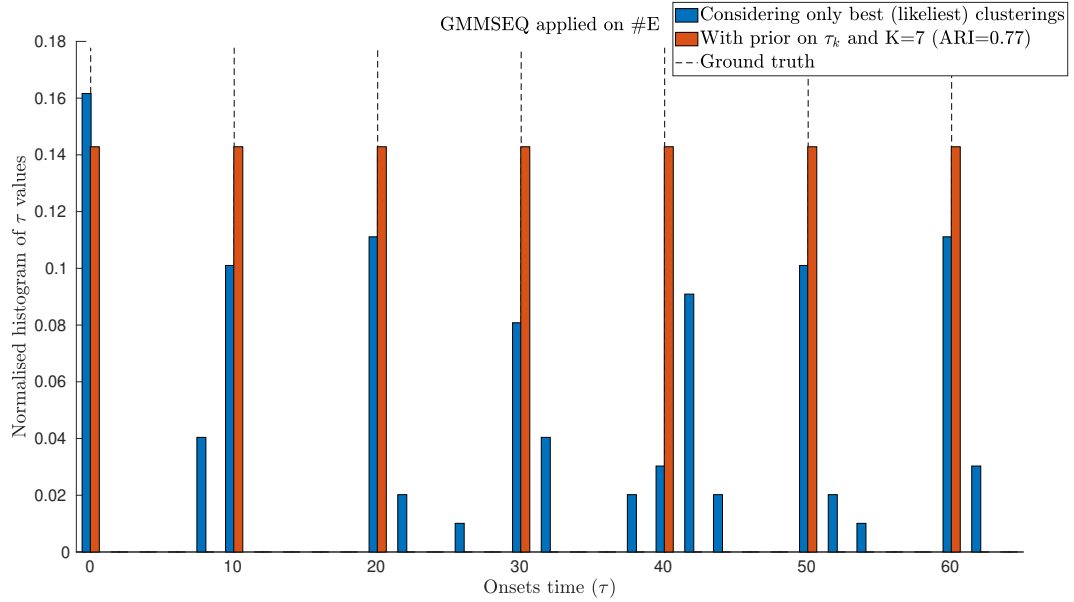


Figure 12: Campaign E: (blue) Histogram of  $\tau_k$  estimates for the three initialization methods and  $K$  ranging from 4 to 14, and (red) histogram with prior on onsets with regularization.

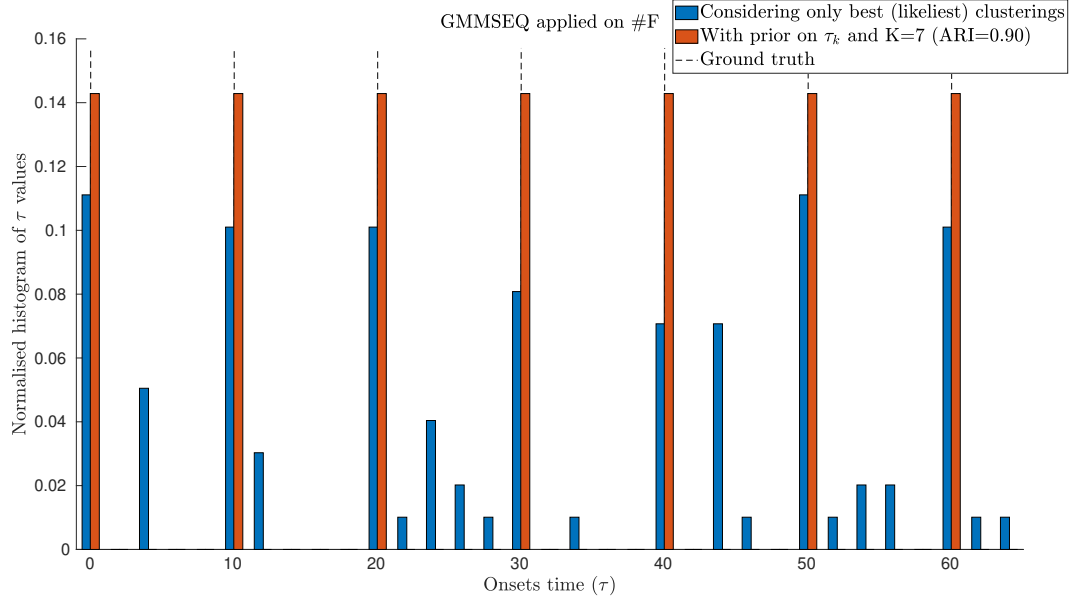


Figure 13: Campaign F: (blue) Histogram of  $\tau_k$  estimates for the three initialization methods and  $K$  ranging from 4 to 14, and (red) histogram with prior on onsets with regularization.

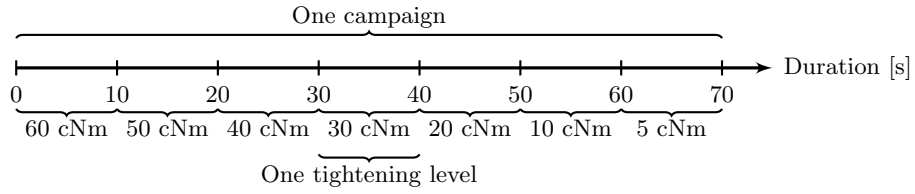


Figure 14: Timeline of tightening levels to interpret the next figures.

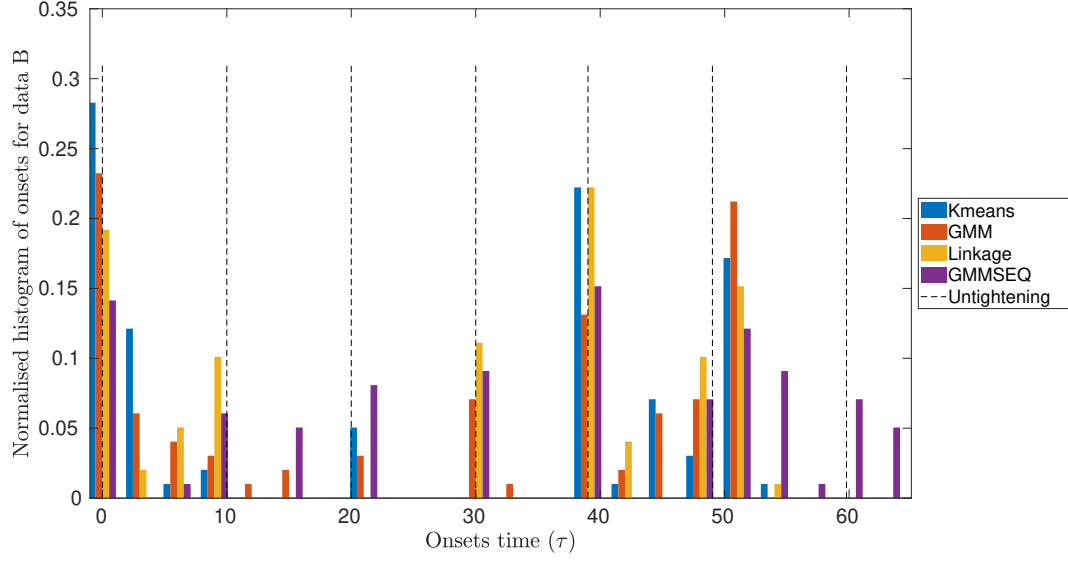
- Campaign B (Figure 9): Levels 60, 40, 30, 20 are precisely detected with a clear peak centered at the correct place. Levels 50, 10 and 5 shows less noticeable peaks but the bins in the histogram show modes that are well positioned around the expected positions.
- Campaign C (Figure 10): For this campaign, a level is missing, which explains why there is no peak around 5 cNm (right-hand side); the levels were indeed shifted by one level in the figure due to one missing level. Figure 10 shows clear peaks at the correct positions. There are also two additional peaks at 25s (30 cNm) and (5 cNm), which may be due to a change in the level during vibration tests.
- Campaigns D (Figure 11) and E (Figure 12): All levels are precisely detected with a clear peak centered at the correct location.
- Campaign F (Figure 13): Levels 60, 50, 40, 20, 10, 5 are precisely detected with a clear peak (or two close peaks) centered at the correct location. For level 30 the peak is less noticeable. Some additional peaks appear around 5 s (middle of the period of 60 cNm) and 43 s (20 cNm), which may be due to a change in the level during vibration tests.

From these figures, it can also be observed that **GMMSEQ** generated onsets with quite similar probability (except for campaign B). The bars in the histogram generally exhibit quite similar values for all tightening levels, which means that the number of AE signals for each tightening level are quite similar. Since the vibration has a fixed frequency independent of the tightening, the sources of AE signals seem to be activated in each cycle (see the streaming and the velocimeter in the top-left part of Figure 1).

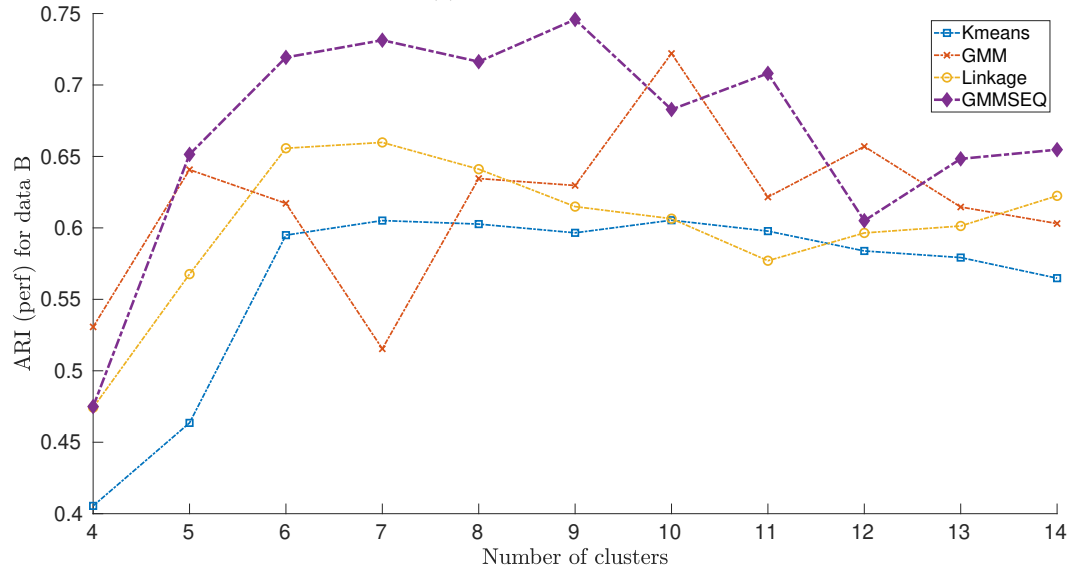
For comparison purposes, Figures 15a to 19a show the histograms of onsets estimated from partitions calculated using the K-means, a standard GMM and hierarchical clustering (HC) using the Ward method (the three implementations are available in the MATLAB Statistics and Machine Learning toolboxes). The K-means algorithm was run 10 times and the model with the smallest sum of squared-distance was selected. GMM was run 10 times with full covariance matrices for each cluster and the model with the highest likelihood was selected. The histograms were normalized for each method independently. We used 4 to 14 clusters as in the previous tests. For these three methods, the onsets are defined by the time of the first occurrence of every cluster. The previous results of **GMMSEQ** are recalled in these figures (see the legend) for direct comparison. As before, the dashed lines represent the times when the tightening was manually changed. The bottom figures represent a quantitative evaluation that will be discussed later on.

The first point to be noticed in Figures 15a to 19a is the levels of the bars (probability of occurrence) around the change of tightening, which are not uniform in contrast to what was observed with **GMMSEQ**. It is the case, for example, for K-means, GMM and HC in campaign B for 60 cNm (0 s) and 20 cNm (40 s), and 10 cNm (50 s), as well as campaigns C (around 10 s - 50 cNm and 30 s - 20 cNm), D (around 10 s - 50 cNm and 20 s - 40 cNm) and F (around 0 s - 60 cNm). The K-means algorithm yields six peaks for campaign F between 0-20 s showing that six clusters are found for only three levels. This result from the K-means also shows that varying the number of clusters does not allow a better discovery of the onsets. In comparison, a uniform distribution of the peaks, as shown by **GMMSEQ**, tends to demonstrate that the onsets are sufficiently sensitive to the number of clusters, which is a good point when we are interested in discovering the timeline, and this sensitivity is not too pronounced so that the onsets are found at the correct location. It



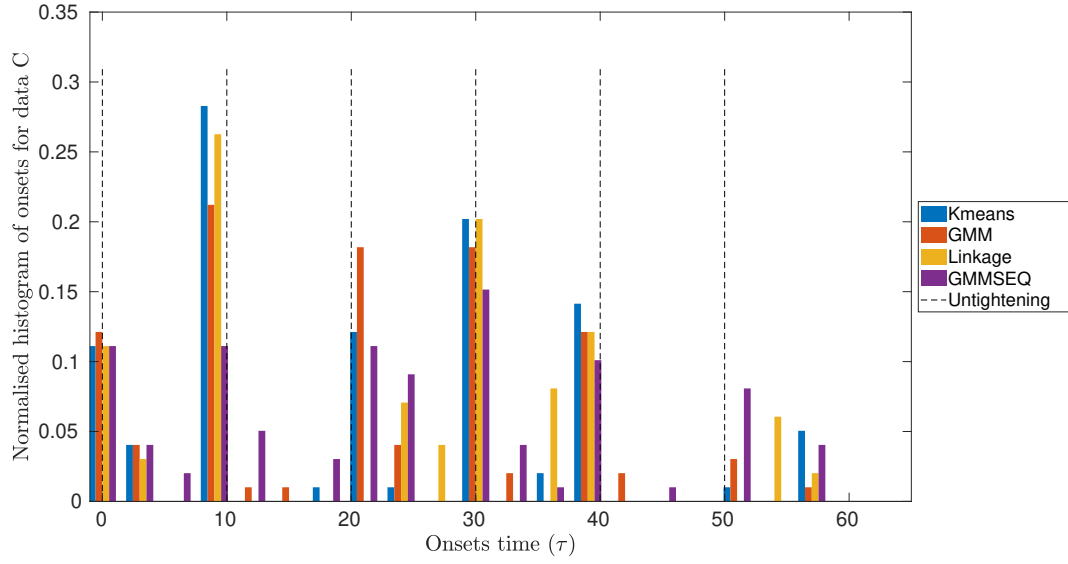


(a) Onset distribution.

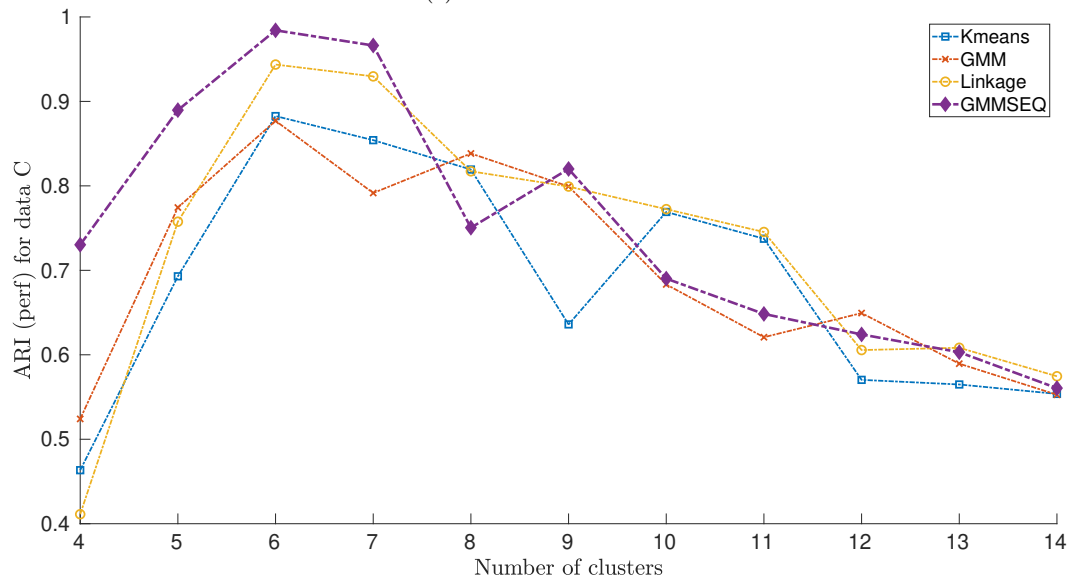


(b) Performance assessed by ARI.

Figure 15: Campaign B: Comparison between standard clustering methods and GMMSEQ.

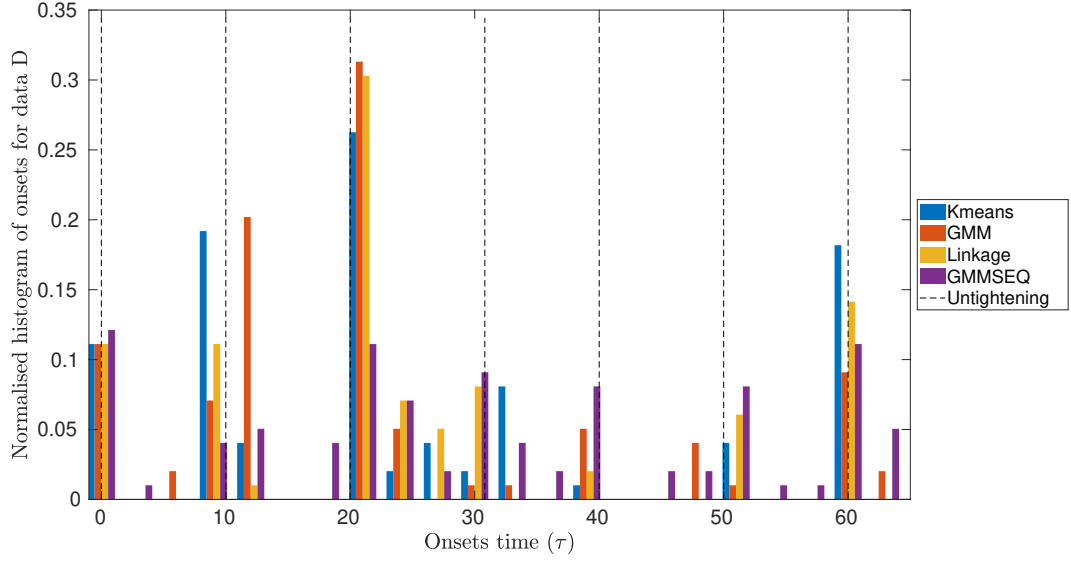


(a) Onsets distribution.

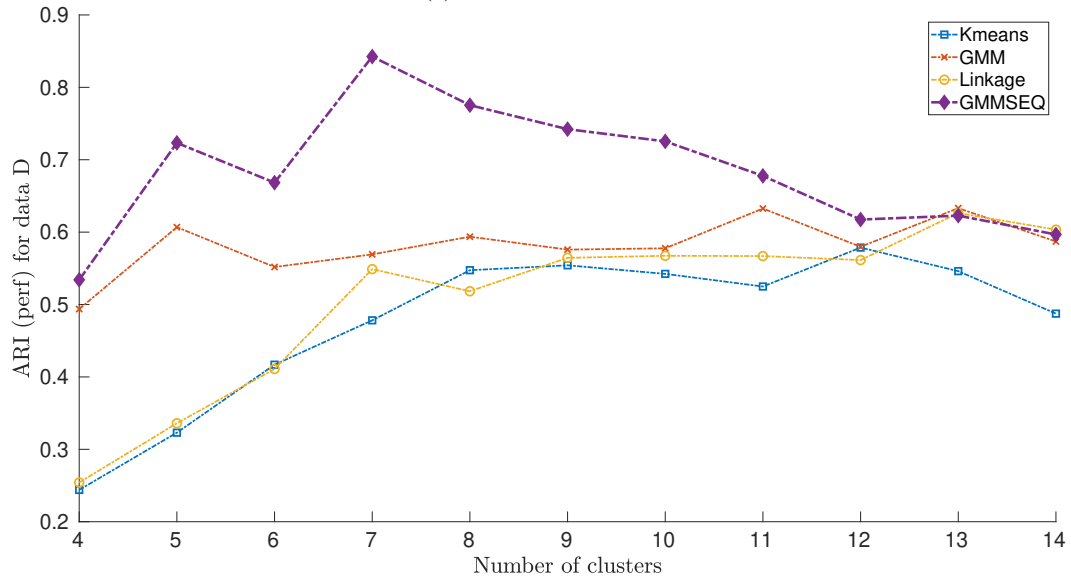


(b) Performance assessed by ARI.

Figure 16: Campaign C: Comparison between standard clustering methods and GMMSEQ.

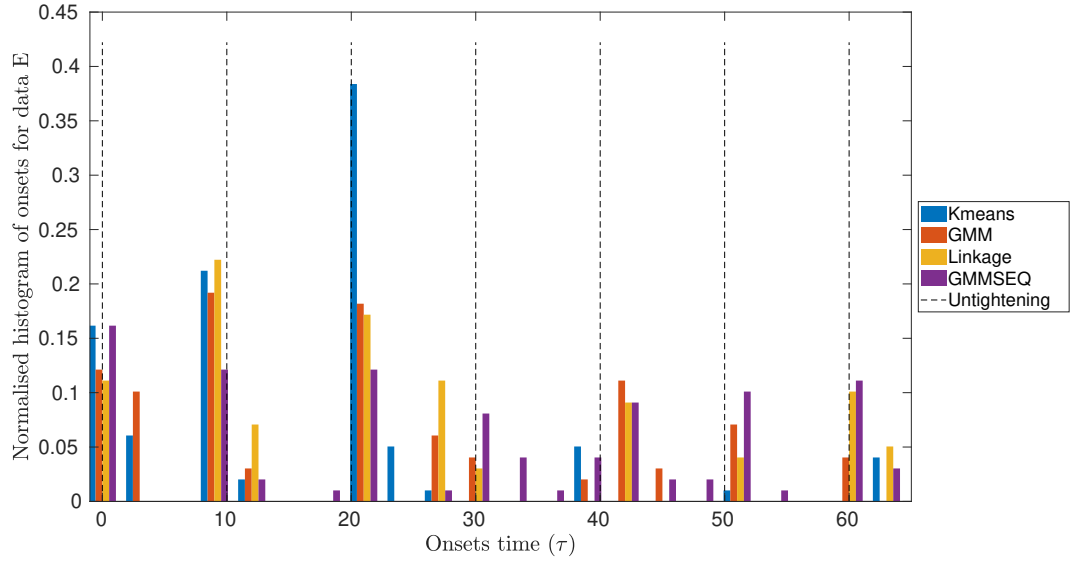


(a) Onsets distribution.

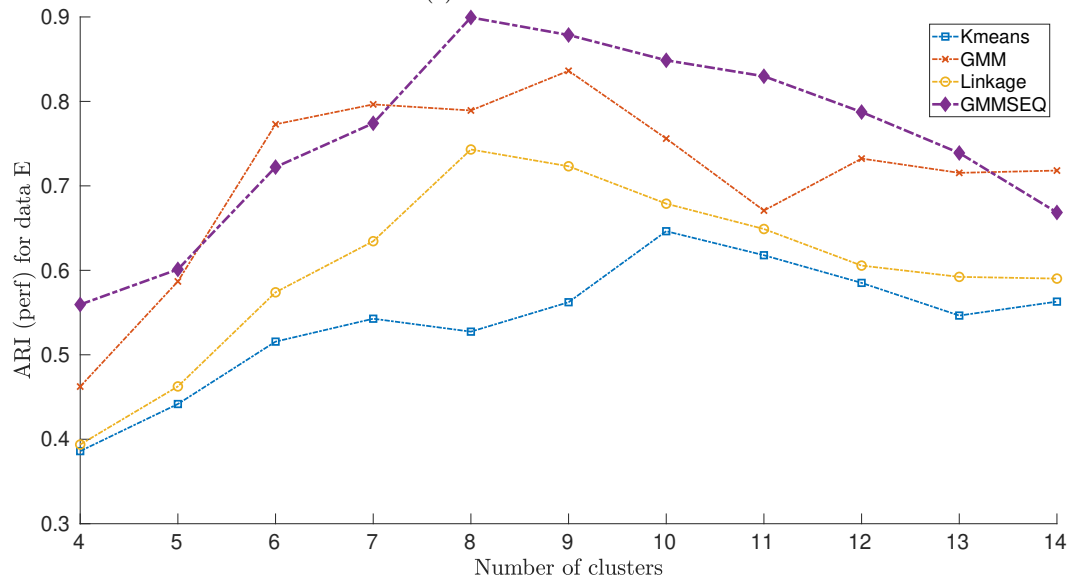


(b) Performance assessed by ARI.

Figure 17: Campaign D: Comparison between standard clustering methods and GMMSEQ.

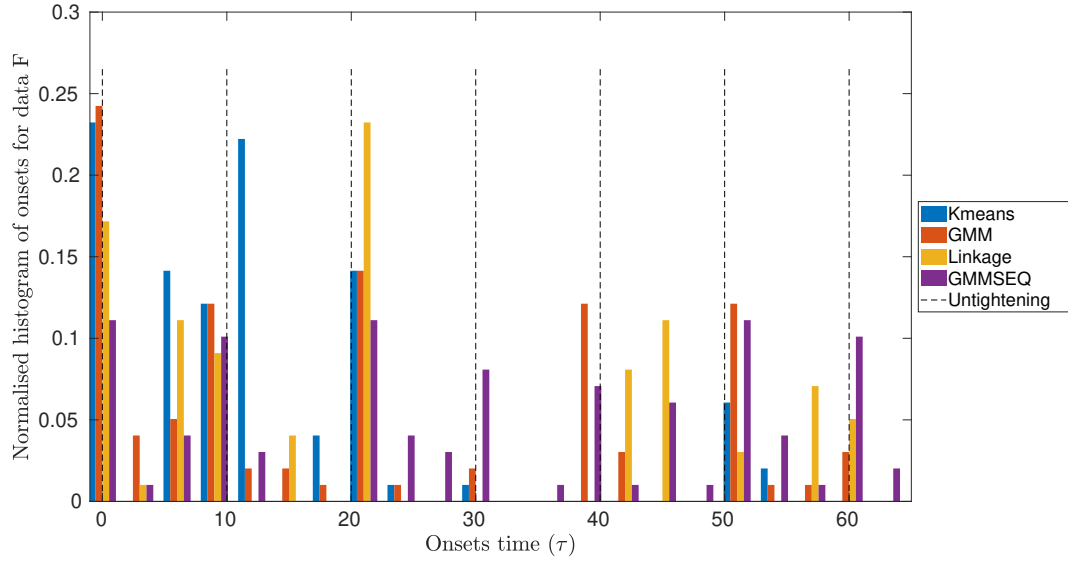


(a) Onsets distribution.

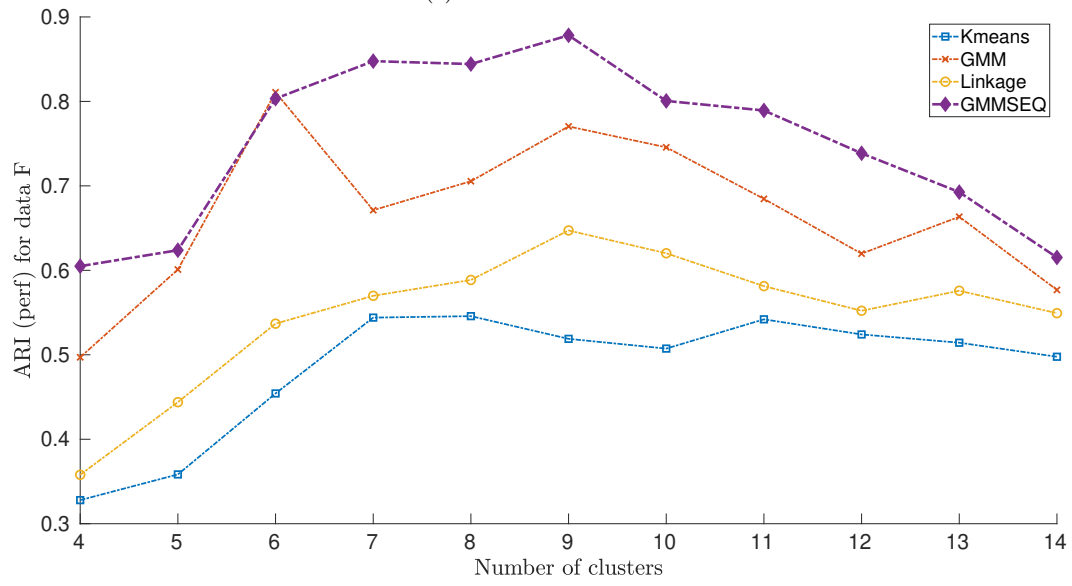


(b) Performance assessed by ARI.

Figure 18: Campaign E: Comparison between standard clustering methods and GMMSEQ.



(a) Onsets distribution.



(b) Performance assessed by ARI.

Figure 19: Campaign F: Comparison between standard clustering methods and GMMSEQ.

can also be observed that the standard methods provide inaccurate estimation of the onsets below or equal to 30 cNm (above 30 s), independently of the dataset (B-F).

The evaluation of onsets is not simple and cannot be precisely performed in a quantitative manner. The qualitative interpretation of histograms provides quite clear information but, in order to quantitatively assess the performance, we used the Adjusted Rand Index [59] (ARI), a corrected-for-chance (and, thus, more severe) version of the Rand Index for clustering evaluation in the presence of a ground truth. In the present case, for the sake of quantitatively evaluating the results against over methods, the tightening levels are supposed to represent a reference to be compared with. For that, we assume that the torque remained close to the level which was set at the beginning of every period of 10 s.

The ARI is displayed in Figures 15b to 19b. This index should normally be maximized for a number of clusters equal to 7 (if the tightening level is really a ground truth) or to 6 for campaign C. The plots with diamond markers represent the ARI for GMMSEQ. For this method, it can be observed that the maximum is generally observed for 6 to 9 clusters which is consistent with the number of tightening levels. The performance of GMMSEQ is also stable with respect to the number of clusters. This comparison confirms the relevance of representing onsets, since the performance of GMMSEQ generally outperforms the standard GMM method, from which it only differs by the use of the sigmoid functions to take account of onsets.

To conclude this experimental section while opening up some perspectives, we illustrate in Figure 20 (right-hand side) the output of non-metric multidimensional scaling (MDS), using Sammon’s nonlinear mapping criterion [60, 61], applied to the means found by GMMSEQ with 14 clusters on campaign B. MDS allows us to visualize, in a two-dimensional space, how close the means are to each other. It is computed from the pairwise Euclidean distances between the means. The grouping of the onsets ( $\tau_k$  values, left-hand side) was made manually based on the assumption that the tightening levels can be used as a reference. Only then, the grouping of the means (right-hand side) was made similarly to the onsets. As observed in previous figures (histograms), the increase of the number of clusters leads to a natural grouping of the onsets. The point that was not emphasized in previous figures, and that appears here, is that the grouping of onsets also implies a natural grouping of the means. Conclusively, it seems that the acoustic emission sources at each tightening level may be represented by a multi-modal distribution made of two components. The clusters do not actually represent AE sources but modes of a more complex distribution. This is coherent with the observations made in Table 1 (see beginning of the Section).

#### 4. Conclusion

The GMMSEQ clustering method introduced in the paper makes it possible to manage continuous timestamps attached to AE signals. This information is exploited during the clustering process allowing one to gain new insights into the AE data streams. Cluster onsets, growth rates and levels of activation through time are estimated together with the parameters of their distributions in the feature space. Therefore, this new clustering method has unique characteristics that stand out from existing methods for AE data interpretation. Although initially developed for AE data, it can be used for time-series analysis in a general way.

The performance of the method has been demonstrated on simulated and real datasets. The latter have allowed us to demonstrate the relevance of the clusters during loosening of bolted joints. The comparison with three standard methods shows that GMMSEQ not only provides

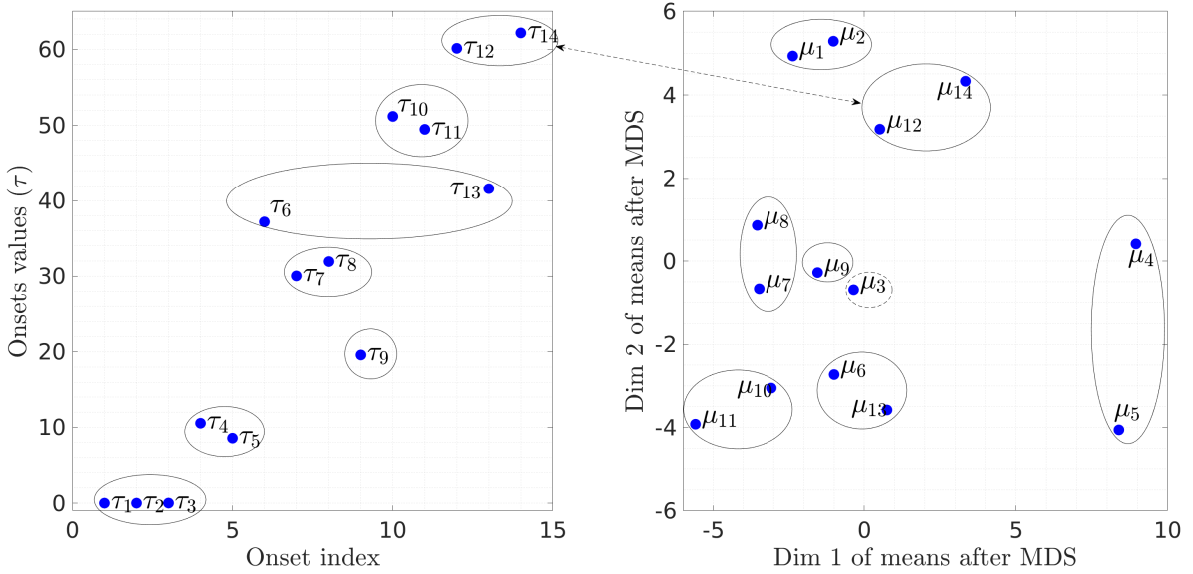


Figure 20: MDS applied to the means of GMMSEQ with 14 clusters on campaign E. Cluster 3 on the right-hand side is surrounded with a dashed circle because the grouping is not as natural as the others (with clusters 1 and 2 according to the onsets).

useful qualitative indications about the timeline of clusters, but also has better performance in terms of cluster characterization.

This work opens up many perspectives. First, the approach can be extended to other mixture models considering non-Gaussian distributions. Our shared code includes, for example, an extension to a mixture of multivariate Student-t distributions, which is not described in this paper.

The possibility to include prior information about the cluster onsets was addressed in the paper using a regularization of the objective function. Prior information about some other parameters such as the cluster centers could be exploited too, which could potentially improve the convergence of the algorithm to “better” estimates with a clear physical interpretation. The possibility of incorporating physical knowledge in the objective function could also be investigated.

Finally, the proposed optimization procedure assumes that all data are available at once (offline or batch analysis). The extension to online clustering with evolving parameters is a possible future direction for application, for example, to structural health monitoring or statistical process control.

## Acknowledgement

This work was partly carried out in the framework of the EIPHI Graduate school (contract ANR-17-EURE-0002) and the project RESEM-COALESCENCE funded by the Institut de Recherche Technologique Matériaux Métallurgie Procédés (IRT M2P) and Agence Nationale de la Recherche (ANR). The authors are also thankful to MIFHySTO and AMETISTE platforms.

## Appendix A. Gradient of $Q$ with respect to $g_k$ , $b_k$ and $\xi_k$

The gradients of the auxiliary function  $Q$  with respect to the variables of interest are given below. We first start by expressing the derivatives with respect to the instrumental variables,

namely  $g_k, b_k, \xi_k$  for each component in the mixture:

$$\frac{\partial Q}{\partial g_k} = \frac{\partial Q}{\partial \gamma_k} \frac{\partial \gamma_k}{\partial g_k} = 2g_k \frac{\partial Q}{\partial \gamma_k}, \quad k = 2, \dots, K \quad (\text{A.1a})$$

$$\frac{\partial Q}{\partial b_k} = \frac{\partial Q}{\partial \beta_k} \frac{\partial \beta_k}{\partial b_k} = 2b_k \frac{\partial Q}{\partial \beta_k}, \quad k = 2, \dots, K \quad (\text{A.1b})$$

$$\frac{\partial Q}{\partial \xi_k} = \frac{\partial Q}{\partial \tau_k} \frac{\partial \tau_k}{\partial \xi_k} = \frac{\partial Q}{\partial \tau_k} \tau_k \left(1 - \frac{\tau_k}{T}\right), \quad k = 2, \dots, K, \quad (\text{A.1c})$$

where (A.1c) uses the following property of the logistic function  $\Lambda(u) = 1/(1 + \exp(-u))$ :  $\Lambda'(u) = \Lambda(u)[1 - \Lambda(u)]$ . The derivatives with respect to  $\beta_k, \gamma_k$  and  $\tau_k$  are given by

$$\frac{\partial Q}{\partial \beta_k} = \sum_{l=1}^K \sum_{i=1}^N \frac{\partial Q}{\partial \pi_{il}} \frac{\partial \pi_{il}}{\partial \alpha_{ik}} \frac{\partial \alpha_{ik}}{\partial \beta_k}, \quad k = 2, \dots, K, \quad i = 1, \dots, N \quad (\text{A.2a})$$

$$\frac{\partial Q}{\partial \gamma_k} = \sum_{l=1}^K \sum_{i=1}^N \frac{\partial Q}{\partial \pi_{il}} \frac{\partial \pi_{il}}{\partial \alpha_{ik}} \frac{\partial \alpha_{ik}}{\partial \gamma_k}, \quad k = 2, \dots, K, \quad i = 1, \dots, N \quad (\text{A.2b})$$

$$\frac{\partial Q}{\partial \tau_k} = \sum_{l=1}^K \sum_{i=1}^N \frac{\partial Q}{\partial \pi_{il}} \frac{\partial \pi_{il}}{\partial \alpha_{ik}} \frac{\partial \alpha_{ik}}{\partial \tau_k}, \quad k = 2, \dots, K, \quad i = 1, \dots, N. \quad (\text{A.2c})$$

We have

$$\frac{\partial Q}{\partial \pi_{il}} = \frac{y_{il}^{(q)}}{\pi_{il}}, \quad l = 1, \dots, K \quad (\text{A.3})$$

and

$$\frac{\partial \pi_{il}}{\partial \alpha_{ik}} = \begin{cases} \frac{\sum_{q=1}^K \alpha_{iq} - \alpha_{il}}{\left(\sum_{q=1}^K \alpha_{iq}\right)^2} & \text{if } k = l \\ \frac{-\alpha_{il}}{\left(\sum_{q=1}^K \alpha_{iq}\right)^2} & \text{if } k \neq l \end{cases} \quad (\text{A.4})$$

for all  $k$  and  $l$  in  $\{1, \dots, K\}$ .

Using the equality  $\alpha_{ik} = \beta_k \Lambda(\gamma_k(t_i - \tau_k))$ , we have

$$\frac{\partial \alpha_{ik}}{\partial \beta_k} = \Lambda(\gamma_k(t_i - \tau_k)) = \frac{\alpha_{ik}}{\beta_k}, \quad (\text{A.5})$$

$$\frac{\partial \alpha_{ik}}{\partial \gamma_k} = \beta_k(t_i - \tau_k) \Lambda'(\gamma_k(t_i - \tau_k)) \quad (\text{A.6a})$$

$$= \alpha_{ik}(t_i - \tau_k) [1 - \Lambda(\gamma_k(t_i - \tau_k))] \quad (\text{A.6b})$$

$$= \alpha_{ik}(t_i - \tau_k) \left[1 - \frac{\alpha_{ik}}{\beta_k}\right], \quad (\text{A.6c})$$

and

$$\frac{\partial \alpha_{ik}}{\partial \tau_k} = -\gamma_k \beta_k \Lambda'(\gamma_k(t_i - \tau_k)) \quad (\text{A.7a})$$

$$= -\gamma_k \alpha_{ik} [1 - \Lambda(\gamma_k(t_i - \tau_k))] \quad (\text{A.7b})$$

$$= -\gamma_k \alpha_{ik} \left[1 - \frac{\alpha_{ik}}{\beta_k}\right]. \quad (\text{A.7c})$$



**Remark 1.** To impose the constraint  $\gamma_1 = \dots = \gamma_K$ , we simply sum the derivatives w.r.t.  $\gamma_k$ :

$$\frac{\partial Q_r}{\partial \gamma} = \sum_{k=1}^K \frac{\partial Q}{\partial \gamma_k},$$

where  $\frac{\partial Q}{\partial \gamma_k}$  is computed using (A.2b).

When considering a prior on onsets, the derivatives w.r.t.  $\tau_k$  (A.2c) become:

$$\frac{\partial Q_r}{\partial \tau_k} = \sum_{l=1}^K \sum_{i=1}^N \frac{\partial Q}{\partial \pi_{il}} \frac{\partial \pi_{il}}{\partial \alpha_{ik}} \frac{\partial \alpha_{ik}}{\partial \tau_k} - 2\lambda \left( \tau_k - \tau_k^{\text{prior}} \right), \quad k = 2, \dots, K, \quad i = 1, \dots, N. \quad (\text{A.8})$$

Algorithm 1 summarises the different steps of the gradient computation.

---

**Algorithm 1** Gradient computation.

---

**Require:**  $\beta_k, \gamma_k, \tau_k, k = 2, \dots, K$   
**for**  $i = 1$  **to**  $N$  **do**  
    **for**  $k = 2$  **to**  $K$  **do**  
        Compute  $\frac{\partial \alpha_{ik}}{\partial \beta_k}$  using (A.5)  
        Compute  $\frac{\partial \alpha_{ik}}{\partial \gamma_k}$  using (A.6)  
        Compute  $\frac{\partial \alpha_{ik}}{\partial \tau_k}$  using (A.7)  
        **for**  $l = 1$  **to**  $K$  **do**  
            Compute  $\frac{\partial \pi_{il}}{\partial \alpha_{ik}}$  using (A.4)  
        **end for**  
    **end for**  
**end for**  
**for**  $k = 2$  **to**  $K$  **do**  
    Compute  $\frac{\partial Q}{\partial \beta_k}$  using (A.2a)  
    Compute  $\frac{\partial Q}{\partial \gamma_k}$  using (A.2b)  
    Compute  $\frac{\partial Q_{ik}}{\partial \tau_k}$  using (A.2c) or (A.8)  
    Compute  $\frac{\partial Q}{\partial b_k}$  using (A.1b)  
    Compute  $\frac{\partial Q}{\partial g_k}$  using (A.1a)  
    Compute  $\frac{\partial Q}{\partial \xi_k}$  using (A.1c)  
**end for**  
**Ensure:** Gradient  $\frac{\partial Q}{\partial \omega} = \left\{ \frac{\partial Q}{\partial b_k}, \frac{\partial Q}{\partial g_k}, \frac{\partial Q}{\partial \xi_k} \right\}_{k=2}^K$

---

## References

- [1] Subcommittee E07.92, Standard terminology for nondestructive examinations, Standard, ASTM International, West Conshohocken, PA (2019).
- [2] Guidance notes on structural monitoring using acoustic emissions, Technical report, American Bureau of Shipping, City Plaza Drive, TX, USA (2016).
- [3] C. Scruby, An introduction to acoustic emission, Journal of Physics E: Scientific Instruments 20 (8) (1987) 946.

- [4] C. Farrar, K. Worden, *Structural Health Monitoring: A Machine Learning Perspective*, John Wiley & Sons, Ltd, 2013.
- [5] J. Awerbuch, F. Leone, D. Ozevin, T.-M. Tan, On the applicability of acoustic emission to identify modes of damage in full-scale composite fuselage structures, *Journal of Composite Materials* 50 (4) (2016) 447–469.
- [6] M. Y. Bhuiyan, J. Bao, B. Poddar, V. Giurgiutiu, Toward identifying crack-length-related resonances in acoustic emission waveforms for structural health monitoring applications, *Structural Health Monitoring* 17 (3) (2018) 577–585.
- [7] Y. He, M. Li, Z. Meng, S. Chen, S. Huang, Y. Hu, X. Zou, An overview of acoustic emission inspection and monitoring technology in the key components of renewable energy systems, *Mechanical Systems and Signal Processing* 148 (2021) 107146.
- [8] J. H. Kurz, C. U. Grosse, H.-W. Reinhardt, Strategies for reliable automatic onset time picking of acoustic emissions and of ultrasound signals in concrete, *Ultrasonics* 43 (7) (2005) 538–546.
- [9] E. Pomponi, A. Vinogradov, A. Danyuk, Wavelet based approach to signal activity detection and phase picking: Application to acoustic emission, *Signal Processing* 115 (2015) 110 – 119.
- [10] D. Bianchi, E. Mayrhofer, M. Gröschl, G. Betz, A. Vernes, Wavelet packet transform for detection of single events in acoustic emission signals, *Mechanical Systems and Signal Processing* 64 (2015) 441–451.
- [11] T. W. Liao, Feature extraction and selection from acoustic emission signals with an application in grinding wheel condition monitoring, *Engineering Applications of Artificial Intelligence* 23 (1) (2010) 74 – 84.
- [12] M. Kharrat, E. Ramasso, V. Placet, M. Boubakar, A signal processing approach for enhanced acoustic emission data analysis in high activity systems: Application to organic matrix composites, *Mechanical Systems and Signal Processing* 70 (2016) 1038–1055.
- [13] R. Madarshahian, P. Ziehl, J. M. Caicedo, Acoustic emission bayesian source location: onset time challenge, *Mechanical Systems and Signal Processing* 123 (2019) 483–495.
- [14] E. Ramasso, P. Butaud, T. Jeannin, F. Sarasini, V. Placet, N. Godin, J. Tirillò, X. Gabrion, Learning the representation of raw acoustic emission signals by direct generative modelling and its use in chronology-based clusters identification, *Engineering Applications of Artificial Intelligence* 90 (2020) 103478.
- [15] S. Kattis, Noesis: Advanced data analysis, pattern recognition & neural networks software for acoustic emission applications, in: *Kolloquium Schallemission, Statusberichte zur Entwicklung und Anwendung der Schallemissionsanalyse*, Vol. 12, Fulda, 2017, pp. 1–8.
- [16] G. Manson, K. Worden, K. Holford, R. Pullin, Visualisation and dimension reduction of acoustic emission data for damage detection, *Journal of Intelligent Material Systems and Structures* 12 (8) (2001) 529–536.
- [17] M. Li, J. H. Yang, Feature selection of acoustic emission signal for the slow-speed and heavy-load equipment, in: *Applied Mechanics and Materials*, Vol. 110, Trans Tech Publ, 2012, pp. 3199–3203.
- [18] D. Doan, E. Ramasso, V. Placet, S. Zhang, L. Boubakar, N. Zerhouni, An unsupervised pattern recognition approach for AE data originating from fatigue tests on polymer–composite materials, *Mechanical Systems and Signal Processing* 64 (2015) 465–478.
- [19] M. G. Sause, *In Situ Monitoring of Fiber-Reinforced Composites: Theory, basic concepts, methods, and applications*, springer series in materials science Edition, Vol. 242, Springer Int. Publishing, 2016.
- [20] E. Ramasso, V. Placet, M. Boubakar, Unsupervised consensus clustering of acoustic emission time-series for robust damage sequence estimation in composites, *IEEE Trans. on Instr. and Meas.* 64 (12) (2015) 3297–3307.
- [21] S. Martin-Del-Campo, F. Sandin, Online feature learning for condition monitoring of rotating machinery, *Engineering Applications of Artificial Intelligence* 64 (2017) 187 – 196.
- [22] R. Fuentes, R. Dwyer-Joyce, M. Marshall, J. Wheals, E. Cross, Detection of sub-surface damage in wind turbine bearings using acoustic emissions and probabilistic modelling, *Renewable Energy* 147 (2020) 776 – 797.
- [23] J. MacQueen, Some methods for classification and analysis of multivariate observations, in: *Proc. of the Fifth Berkeley Symposium on Math., Stat. and Prob.*, Vol. 1, 1967, pp. 281–296.
- [24] M. Chai, J. Zhang, Z. Zhang, Q. Duan, G. Cheng, Acoustic emission studies for characterization of fatigue crack growth in 316ln stainless steel and welds, *Applied Acoustics* 126 (2017) 101–113.
- [25] J. C. Dunn, A fuzzy relative of the isodata process and its use in detecting compact well-separated clusters, *Journal of Cybernetics* 3 (1973) 32–57.
- [26] S. N. Omkar, S. Suresh, T. R. Raghavendra, V. Mani, Acoustic emission signal classification using fuzzy c-means clustering, in: *Proceedings of the 9th International Conference on Neural Information Processing, 2002. ICONIP '02.*, Vol. 4, 2002, pp. 1827–1831 vol.4. doi:10.1109/ICONIP.2002.1198989.
- [27] D. E. Gustafson, W. C. Kessel, Fuzzy clustering with a fuzzy covariance matrix, in: *1978 IEEE conference on decision and control including the 17th symposium on adaptive processes*, IEEE, 1979, pp. 761–766.
- [28] G. J. McLachlan, K. E. Basford, *Mixture models. Inference and applications to clustering*, Vol. 84, Marcel

- Dekker, Statistics: Textbooks and Monographs, New York, United States, 1988.
- [29] H. A. Sawan, M. E. Walter, B. Marquette, Unsupervised learning for classification of acoustic emission events from tensile and bending experiments with open-hole carbon fiber composite samples, *Composites Science and Technology* 107 (2015) 89–97.
  - [30] M. Kaminski, F. Laurin, J. Maire, C. Rakotoarisoa, E. Hémon, Fatigue damage modeling of composite structures: the onera viewpoint, *AerospaceLab* 6 (9) (2015) 1–12.
  - [31] A. Saxena, K. Goebel, C. C. Larrosa, V. Janapati, S. Roy, F.-K. Chang, Accelerated aging experiments for prognostics of damage growth in composite materials, Tech. rep., NATIONAL AERONAUTICS AND SPACE ADMINISTRATION, MOFFETT FIELD CA AMES RESEARCH (2011).
  - [32] T. W. Liao, Clustering of time series data - a survey, *Pattern recognition* 38 (11) (2005) 1857–1874.
  - [33] T.-C. Fu, A review on time series data mining, *Engineering Applications of Artificial Intelligence* 24 (1) (2011) 164–181.
  - [34] A. Belhadi, Y. Djenouri, K. Nørvåg, H. Ramampiaro, F. Massegli, J. C.-W. Lin, Space-time series clustering: Algorithms, taxonomy, and case study on urban smart cities, *Engineering Applications of Artificial Intelligence* 95 (2020) 103857.
  - [35] C. S. Möller-Levet, F. Klawonn, K.-H. Cho, O. Wolkenhauer, Fuzzy clustering of short time-series and unevenly distributed sampling points, in: *International symposium on intelligent data analysis*, Springer, 2003, pp. 330–340.
  - [36] M. Sause, A. Gribov, A. Unwin, S. Horn, Pattern recognition approach to identify natural clusters of acoustic emission signals, *Pattern Reco. Lett.* 33 (2012) 17–23.
  - [37] N. Godin, P. Reynaud, G. Fantozzi, *Acoustic emission and durability of composites materials*, ISTE-Wiley editions, 2018.
  - [38] S. Huguet, N. Godin, R. Gaertner, L. Salmon, D. Villard, Use of acoustic emission to identify damage modes in glass fibre reinforced polyester, *Composites Science and Technology* 62 (10–11) (2002) 1433 – 1444.
  - [39] A. Monti, A. El Mahi, Z. Jendli, L. Guillaumat, Mechanical behaviour and damage mechanisms analysis of a flax-fibre reinforced composite by acoustic emission, *Composites Part A: Applied Science and Manufacturing* 90 (2016) 100–110.
  - [40] T. Shiraiwa, K. Ishikawa, M. Enoki, I. Shinozaki, S. Kanazawa, Acoustic emission analysis using bayesian model selection for damage characterization in ceramic matrix composites, *Journal of the European Ceramic Society* 40 (8) (2020) 2791 – 2800.
  - [41] C. Allen, Comparison of the semi-logarithmic with the cumulative chain percentage chart, *School of Science and Mathematics* 38 (1938) 444–450.
  - [42] E. Ramasso, V. Placet, R. Gouriveau, M. Boubakar, Health assessment of composite structures in unconstrained environments using partially supervised pattern recognition tools, in: *Annual Conference of the Prognostics and Health Management Society*, Minneapolis, USA, 2012, pp. 17–27.
  - [43] E. Ramasso, X. Gabrion, D. Doan, M. Kharrat, V. Placet, L. Boubakar, Reconnaissance des sources acoustiques dans les composites à matrice organique: quel(s) critère(s) utiliser pour une classification non-supervisée des signaux?, in: *Congrès Français d’Acoustique, Société Française d’Acoustique*, 2014, pp. 1611–1617.
  - [44] N. Chandarana, Combining passive and active methods for damage mode diagnosis in tubular composites, Ph.D. thesis, Manchester University, Faculty of Science and Engineering, Departement of Materials (11/18/2019).
  - [45] B. Verdin, G. Chevallier, E. Ramasso, ORION-AE: Multisensor acoustic emission datasets reflecting supervised untightening of bolts in a jointed vibrating structure, Data-in-Brief Co-submitted, 2021.
  - [46] B. Verdin, G. Chevallier, E. Ramasso, ORION-AE: Multisensor acoustic emission datasets reflecting supervised untightening of bolts in a jointed vibrating structure (Harvard Dataverse, 2021). doi:10.7910/DVN/FBRDU0.
  - [47] E. P. Frigieri, P. H. Campos, A. P. Paiva, P. P. Balestrassi, Joao, A mel-frequency cepstral coefficient-based approach for surface roughness diagnosis in hard turning using acoustic signals and gaussian mixture models, *Applied Acoustics* 113 (2016) 230 – 237.
  - [48] P. R. Prem, A. R. Murthy, Acoustic emission monitoring of reinforced concrete beams subjected to four-point-bending, *Applied Acoustics* 117 (2017) 28 – 38.
  - [49] R. V. Sagar, J. Srivastava, R. Singh, A probabilistic analysis of acoustic emission events and associated energy release during formation of shear and tensile cracks in cementitious materials under uniaxial compression, *Journal of Building Engineering* 20 (2018) 647 – 662.
  - [50] A. K. Das, D. Suthar, C. K. Leung, Machine learning based crack mode classification from unlabeled acoustic emission waveform features, *Cement and Concrete Research* 121 (2019) 42 – 57.
  - [51] A. Dempster, N. Laird, D. Rubin, Maximum likelihood from incomplete data via the EM algorithm, *Journal of the Royal Statistical Society* 39 (1) (1977) 1–38.

- [52] G. J. McLachlan, T. Krishnan, *The EM Algorithm and Extensions*, 2nd Edition, Wiley, New York, 2008.
- [53] C. Bishop, *Pattern Recognition and Machine Learning*, Springer, 2006.
- [54] C. Biernacki, G. Govaert, Choosing models in model-based clustering and discriminant analysis, *Journal of Statistical Computation and Simulation* 64 (1) (1999) 49–71.
- [55] J.-P. Baudry, A. E. Raftery, G. Celeux, K. Lo, R. Gottardo, Combining mixture components for clustering, *Journal of computational and graphical statistics* 19 (2) (2010) 332–353.
- [56] G. Chevallier, E. Ramasso, P. Butaud, Detection and analysis of loosening in jointed structures using acoustic emission sensors and smart bolts, in: *37th Int. Conference on Modal Analysis*, Florida, USA, 2019, pp. 1–3.
- [57] Z. Zhang, Y. Xiao, Z. Su, Y. Pan, Continuous monitoring of tightening condition of single-lap bolted composite joints using intrinsic mode functions of acoustic emission signals: a proof-of-concept study, *Structural Health Monitoring* 18 (4) (2019) 1219–1234.
- [58] S. Gonzalez Andino, R. Grave de Peralta Menendez, G. Thut, L. Spinelli, O. Blanke, C. Michel, T. Landis, Measuring the complexity of time series: an application to neurophysiological signals, *Human brain mapping* 11 (1) (2000) 46–57.
- [59] N. Vinh, J. Epps, J. Bailey, Information theoretic measures for clusterings comparison: Is a correction for chance necessary?, in: *Proc. of the 26th Annual Int. Conference on Machine Learning*, ACM, New York, NY, USA, 2009, pp. 1073–1080.
- [60] J. W. Sammon, A nonlinear mapping for data structure analysis, *IEEE Transactions on computers* 100 (5) (1969) 401–409.
- [61] B. Ghoggh, A. Ghodsi, F. Karray, M. Crowley, Multidimensional scaling, sammon mapping, and isomap: Tutorial and survey, *arXiv preprint arXiv:2009.08136*.